

AD-A178 782

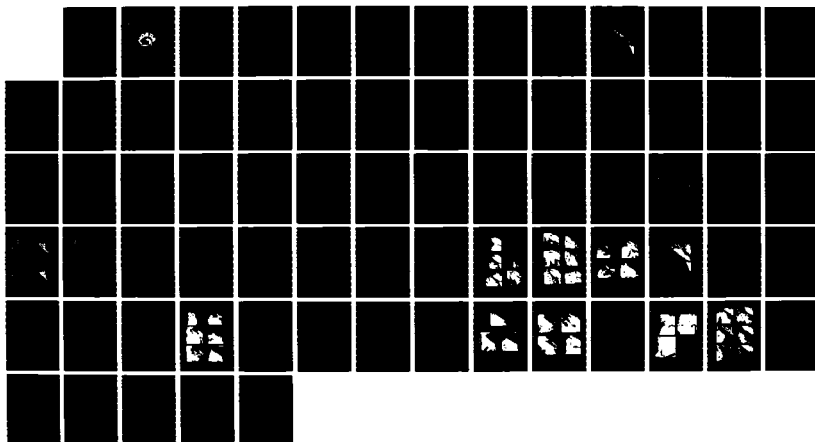
PHYSICAL OCEANOGRAPHY OF THE CONTINENTAL SHELF REGION  
OFF JUAN DE FUCA STRAIT(U) NAVAL OCEAN RESEARCH AND  
DEVELOPMENT ACTIVITY NSTL STATION NS M J EMERY MAY 84  
NORDA-TN-231

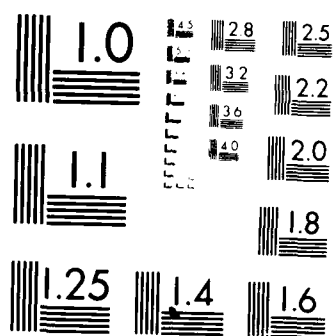
1/1

UNCLASSIFIED

F/G 8/10

NL





MICROCOPY RESOLUTION TEST CHART  
NATIONAL BUREAU OF STANDARDS-1963-A

AD-A170 702

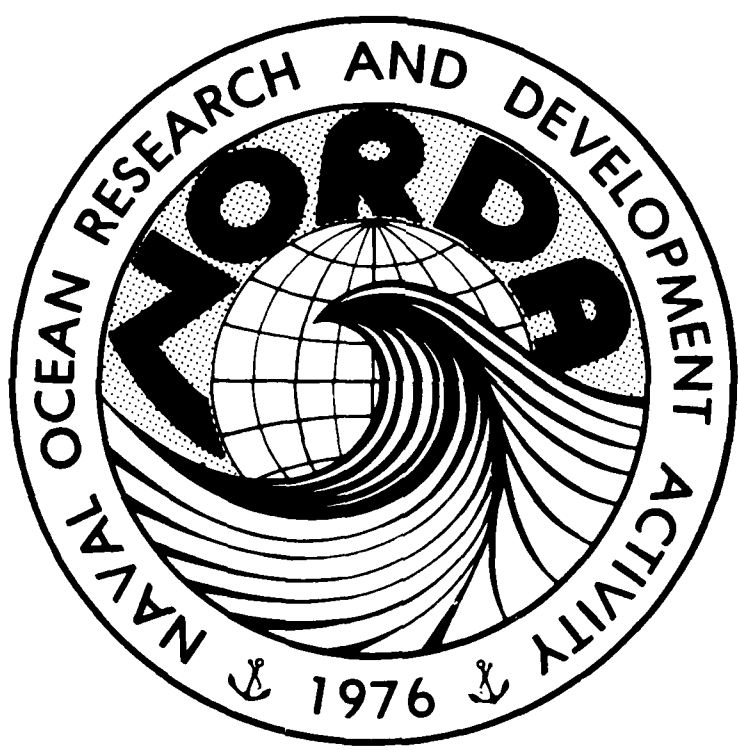
Naval Ocean Research and  
Development Activity  
NSTL, Mississippi 39529



NORDA Technical Note 231

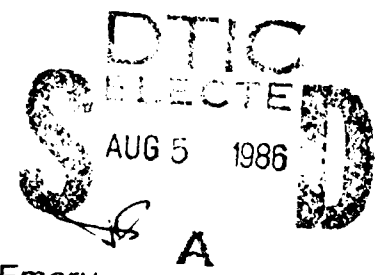


# Physical Oceanography of the Continental Shelf Region off Juan de Fuca Strait



DTIC FILE COPY

Approved for Public Release  
Distribution Unlimited



Prepared by William J. Emery  
For: Ocean Science Directorate  
Applied Oceanography and Geophysics Division

May 1984

86 8 4 137


## Abstract

Through interpretation of observations, a review of the water mass structure and circulation of the ocean just west of the Strait of Juan de Fuca was accomplished. The region of interest ( $47-49^{\circ}\text{N}$ ,  $124-127^{\circ}\text{W}$ ) is influenced both by local and remote forces. External influences are the inflow of fresh water from the Strait of Juan de Fuca, the intrusion of temperature minimum water from the north and west, and the extension of the California Undercurrent into the area, except in spring. Local processes of importance are both wind and topographically produced upwelling and the formation of eddies and meanders through baroclinic instability.

These forces combine to produce the seasonal patterns of mean currents with all southward flow in the spring, southward surface current over a northward undercurrent in summer and fall, and all northward flow in the winter. Meanders, formed by baroclinic instability associated with these current structures, vary from 125-km features in winter and spring to a transition from 75-km to 150-km features in summer. Linear dynamics seem to hold in winter and spring while nonlinear processes are active in summer-fall, when the shorter scale features are stimulated by bottom topography.

In terms of sound velocity the primary concern stems from the intrusions of temperature minima which form shallow surface ducts. Dependent on the vertical salinity structure these minima (and hence sound channels) are usually located between 100 and 200 m coincident with halocline (maximum salinity gradient). It is unlikely that these features form locally but rather advect into the region from the west and north with the surface current. Thus new temperature minima can only

arrive in spring, summer, and early fall when the surface current is southward. In winter flow is everywhere from the south advecting in warm water rather than cold. Temperature maxima, however, are not frequently observed. In winter vertical mixing may also form surface sound velocity ducts.

	
A. ... ..	
... .. or	
Dist. ... ..	
A-1	... ..



# PHYSICAL OCEANOGRAPHY OF THE CONTINENTAL SHELF REGION OFF JUAN DE FUCA STRAIT

## Introduction

The primary purpose of this paper is to provide a succinct and nontechnical review of the water mass structure and circulation of the ocean just west of the Strait of Juan de Fuca. The report will draw on both older published material and the results of new, on-going research. Some effort will be made to translate the discussion of property and current variations into their effects on the vertical sound velocity profile. The level of presentation assumes some degree of familiarity with the basic terms used in physical oceanography but will appeal not only to experts in the field. The text will try to interpret observations rather than merely report them.

While some discussion will be given to the entire eastern North Pacific, most of the work will focus on the area within 47-49°N and 124-127°W. This region is just to the west of the Strait of Juan de Fuca which separates the Olympic Peninsula from Vancouver Island. Existing studies of this region fall into three categories. First there are the early programs (before 1960) designed to evaluate the physical environment for fisheries work in the entire eastern North Pacific. Measurements in the particular area of interest were relatively few in number as the sampling grids were quite coarse. The second category includes a few studies over the past two decades which look more closely at the circulation in this region. Different goals were associated with each project and no comprehensive survey was carried out.

A third group covers more recent comprehensive measurement programs, which include both moored current meter observations and shipboard density measurements. These have provided a much more detailed picture of the circulation over the Continental Shelf. In addition analyses of infrared satellite imagery, in conjunction with time-dependent numerical models, have yielded some valuable insights into the dynamics of the mesoscale (~100 km) fluctuations which occur in the mean coastal currents. As expected these studies reveal that the region exhibits a large amount of variability on both seasonal (annual) and inter-annual (year-to-year) time-scales. These variations largely determine the oceanographic conditions at any particular time (and place) and must, therefore, be considered in describing environmental effects.

#### Bathymetry

Compared to the coastline farther south the Continental Shelf, off Juan de Fuca Strait, is fairly wide (Fig. 1). The 200-m depth contour extends out beyond 70 km from the coast, in this region, compared to 15 km off Pt. Conception (Hickey, 1979). In more detail the 183-m contour of Figure 2 (dashed line) reveals the presence of a topographic trough running up into the mouth of Juan de Fuca Strait. Identified as Juan de Fuca Canyon in Figure 3 this feature is connected to a smaller "Spur Canyon" which turns north intruding into the Continental Shelf. The importance of these topographic features in determining coastal temperature and circulation conditions will be stressed later. Also the role of the canyon in providing a conduit carrying water from the Strait of Juan de Fuca will be discussed.

Some of the shallower topographic features of the Continental Shelf are also represented in Figure 3. La Perouse Bank is a region of summer fishing activity. The

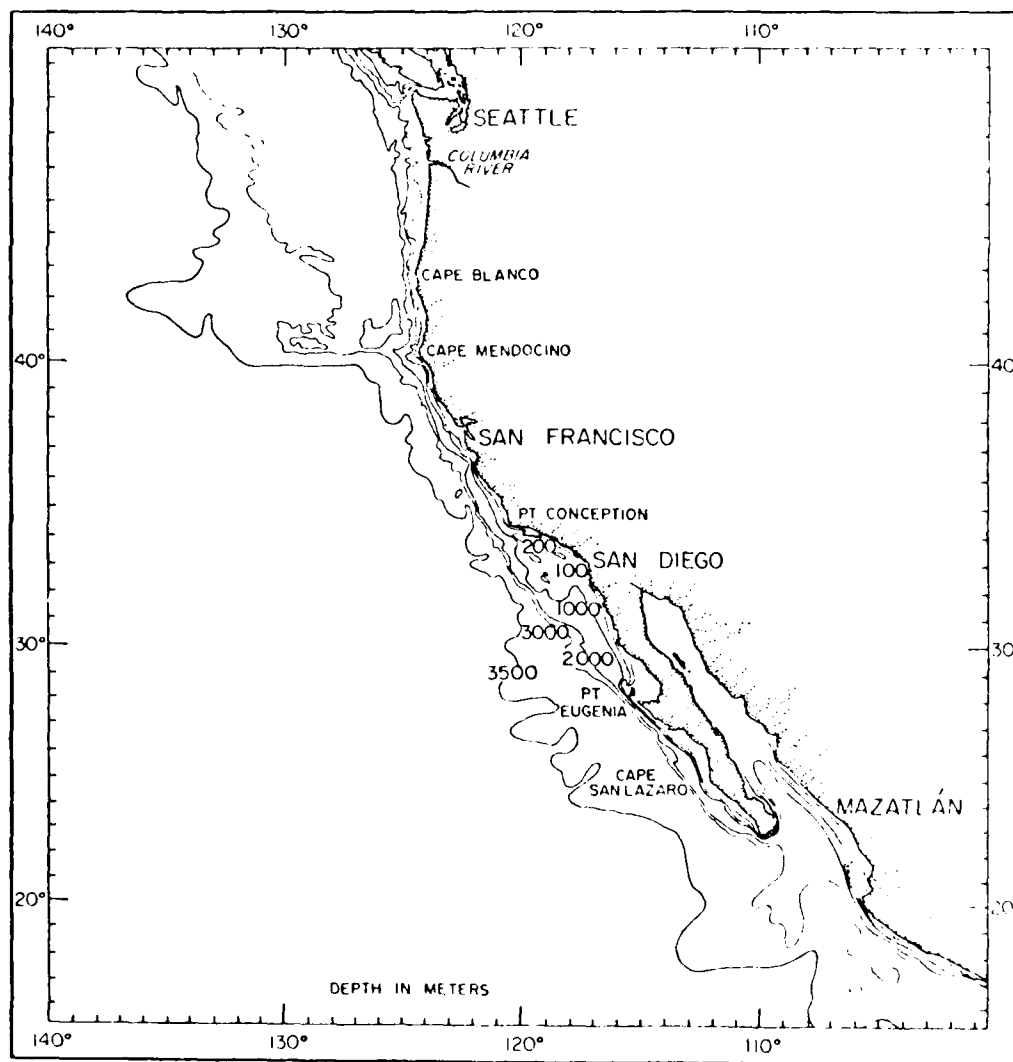


Figure 1. Bottom topography off the west coast of North America



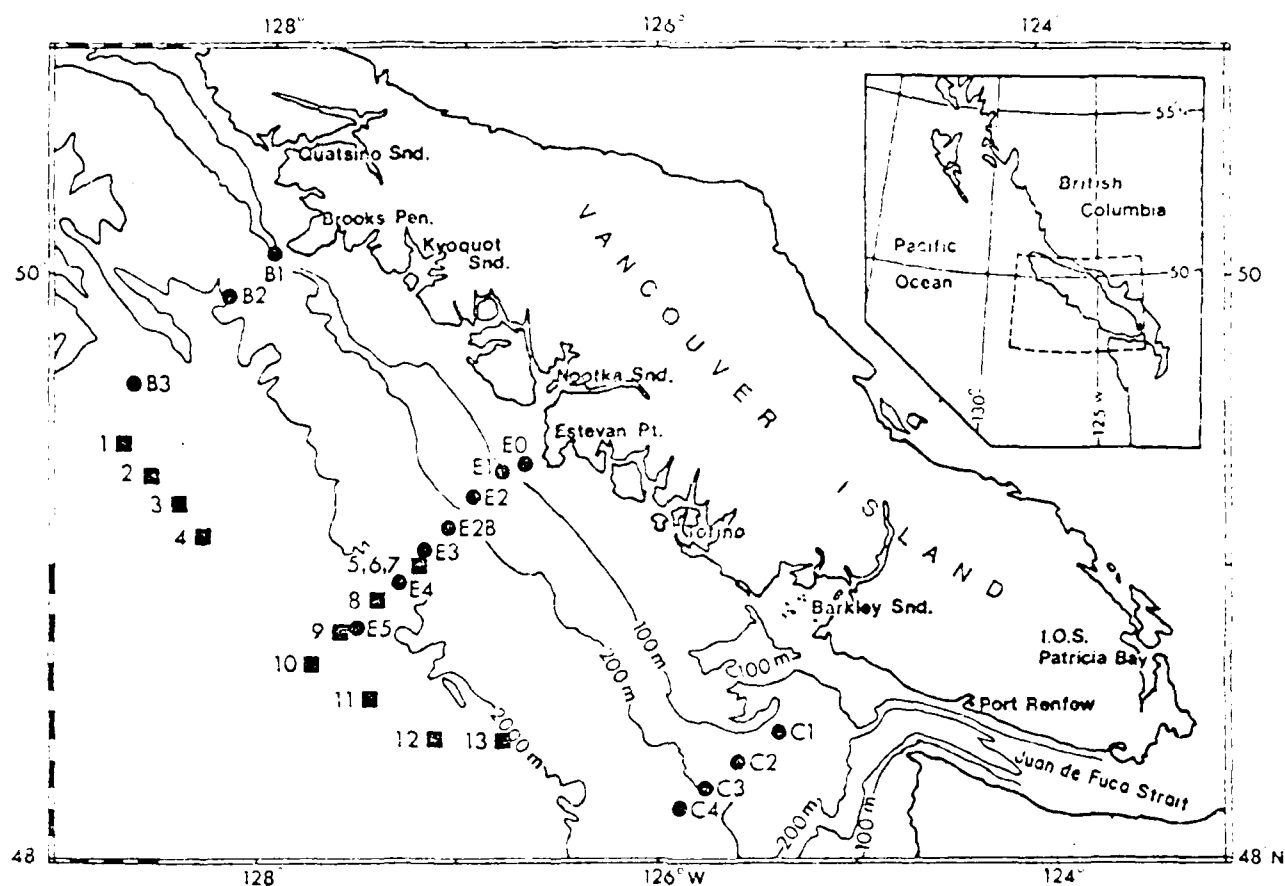


Figure 2. Bottom topography off Vancouver Island

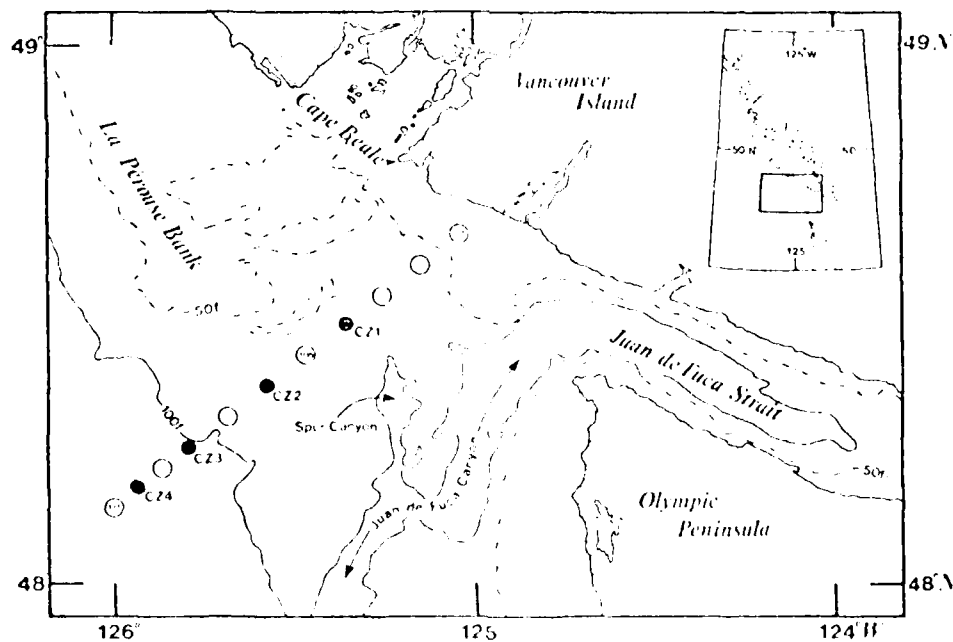


Figure 3. The study region off southern Vancouver Island. Circles mark the CTD locations constituting line 1, stations 101 to 111, the darkened circles are also mooring locations. To a good approximation the shelf edge is delineated by the 100-fathom (180 m) contour.

50-fathom contour also emphasizes the steepness in Juan de Fuca Canyon by its proximity to the 100-fathom line.

On a much larger scale the alongshore regularity of the coastal features on the west coast of Vancouver Island should be mentioned. As shown in Figure 4 there is a series of promontories extending seaward starting at Brooks Peninsula. Extrapolated offshore to the continental shelf break these promontories, and the associated canyons, lead to the gentle undulations of the 200-m isobath in Figure 4 (left). These topographic features have a length scale of about 75 km alongshore. As will be discussed these topographic variations act to initiate current meanders, in the coastal circulation, that eventually form mesoscale eddies.

#### Water mass structure

As presented in the climatological curves of Emery and Dewar (1982) the mean TS curve (Fig. 5a) exhibits all of its salinity gradient between 1.5 and 8°C. This emphasizes the fact that the water column seldom warms up above 6°C as revealed by the mean temperature profile of Figure 5b. Here only the upper 100 m experiences temperatures greater than 7°C. There is an important inflection in slope between 100 and 200 m. Here the temperature profile becomes isothermal (constant temperature). This likely reflects the intrusion of temperature minimum water into the region (Roden, 1964).

The temperature gradient is very small below 2000 m where conditions become almost isothermal. The mean salinity gradient is a bit more apparent (Fig. 5c) at these depths. The strongest salinity gradient is, however, between 100 and 250 m consistent with the temperature profile. It is interesting that the temperature

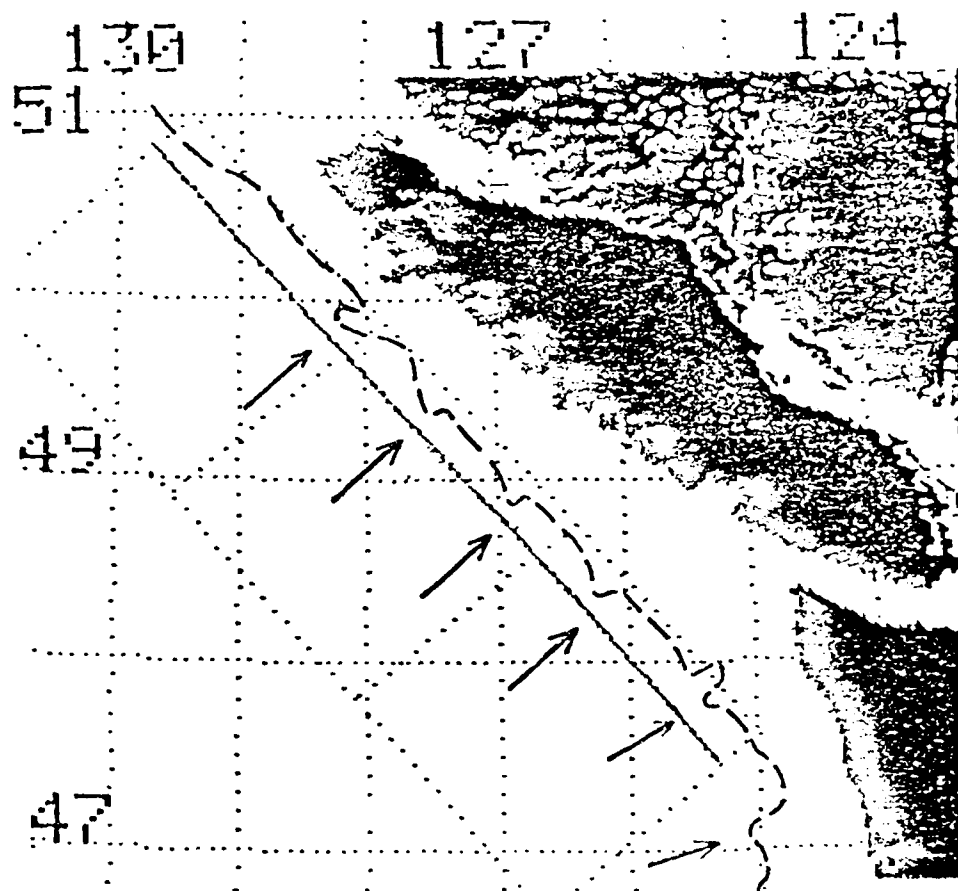


Figure 4. Coastal outline and contours of Continental Shelf break  
(dashed line=183-m contour)

PACIFIC TS AREA # 24  
NUMBER OF STATIONS : 7038

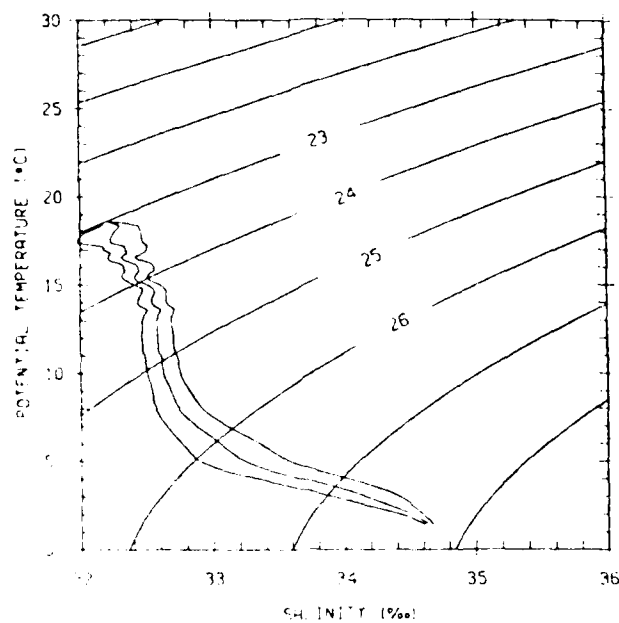


Fig. 5(a)

PACIFIC TZ AREA # 17  
NUMBER OF STATIONS : 4352

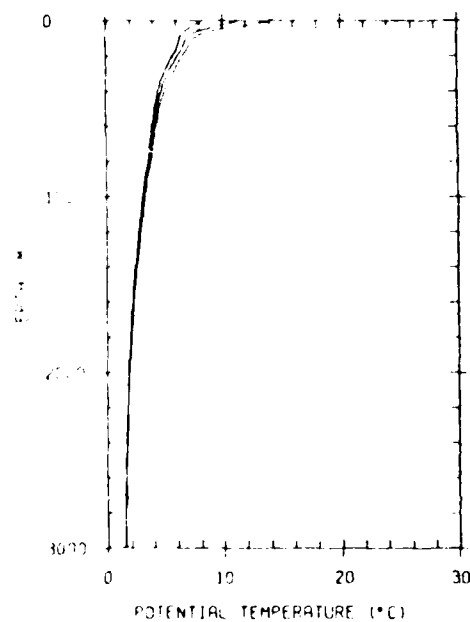


Fig. 5(b)

PACIFIC SZ AREA # 3  
NUMBER OF STATIONS : 411

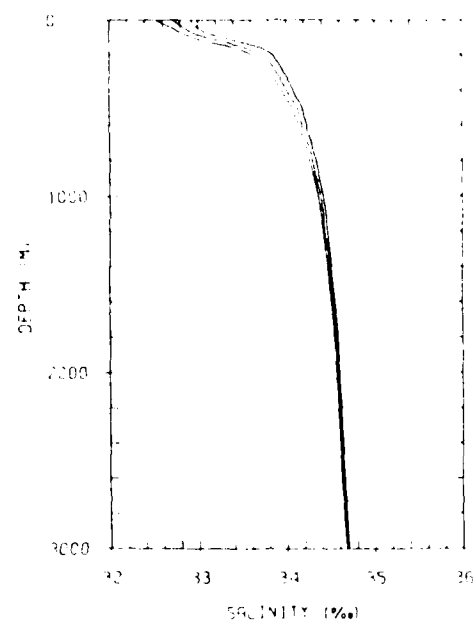


Fig. 5(c)

Figure 5. Mean property curves off Juan de Fuca Strait. Central line represents mean relationship bracketed by standard deviation.

standard deviation becomes quite small at about 500 m while the salinity deviation extends on down below 1000 m. This suggests the importance of salinity variations in this region, one strongly influenced by coastal runoff and outflow from Juan de Fuca Strait.

The effect of this outflow can be seen in zonal sections along 47 and 48°N from 1955-59 as presented in Figure 6. In each year salinity is lowest at the surface just seaward of the Continental Shelf (marked by the black boundary on the right). In these sections the complimentary effects of temperature and salinity are clearly apparent. The temperature sections contain strong thermoclines (maximum temperature gradients) around 50 m, while the salinity sections have the haloclines (maximum salinity gradients) located just below 100 m. Thus the density gradient (pycnocline) combines both the temperature and salinity effects. It is the presence of the salinity gradient, just below 100 m, that allows a thermal inversion to often exist at this depth (Barnett, 1959).

All of the sections demonstrate the shoaling of both the isotherms and isohalines (constant salinity lines) over the Continental Shelf boundary. A strong inter-annual variation can be seen by comparing the summer section from 1957 with those from 1956/9. In 1957 a dramatic warming event occurred increasing temperatures all along the west coast. This can be seen in Figure 6 by comparing the temperature section from 1957 (Fig. 6c) with that from 1956 (Fig. 6b). In 1957 even the 8°C isotherm turns down at the coast to go below 100 m. In 1955/6 the 8°C, and even the 7°C, isotherms turn up towards the surface. This upward turn is also true of the salinity section for these first two years. By comparison the salinity sections from 1957/9 turn up only slightly. It is interesting to note that a coastal warming

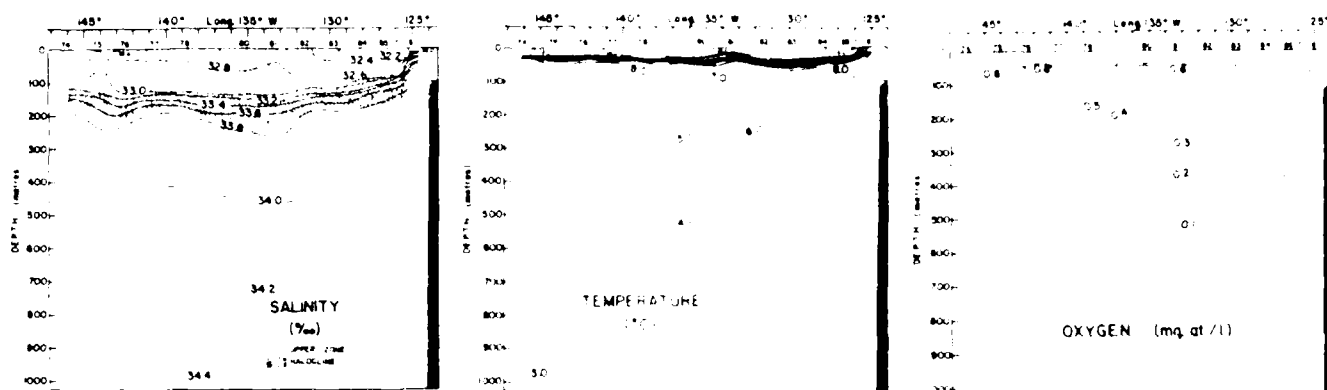


Figure 6a. Vertical sections of salinity, temperature, and dissolved oxygen along approximately latitude 17°N., summer 1955

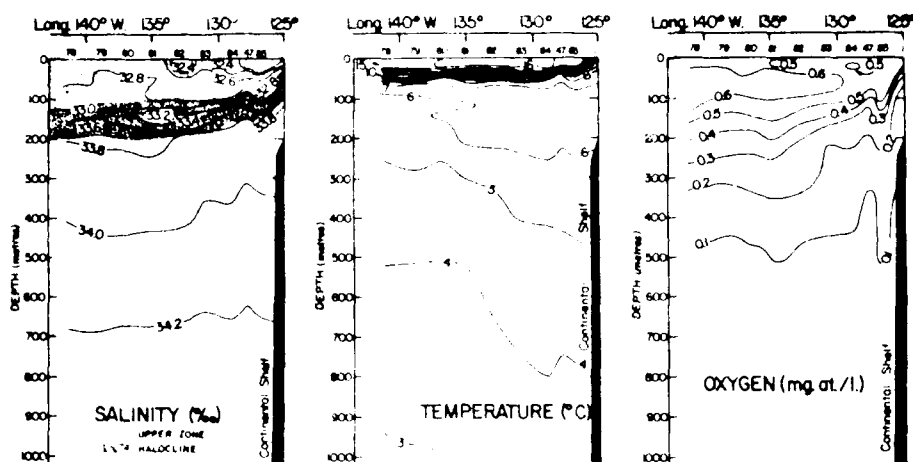


Figure 6b. Vertical sections of salinity, temperature, and dissolved oxygen along approximately latitude 45°N., summer 1956

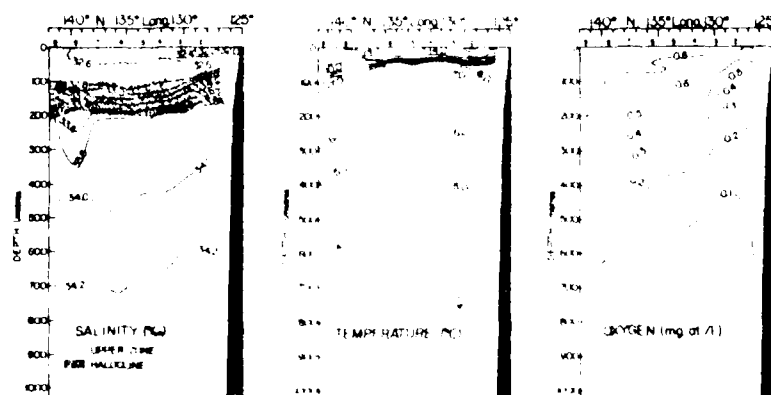


Figure 6c. Vertical sections of salinity, temperature, and dissolved oxygen along approximately latitude 17°N., summer 1957

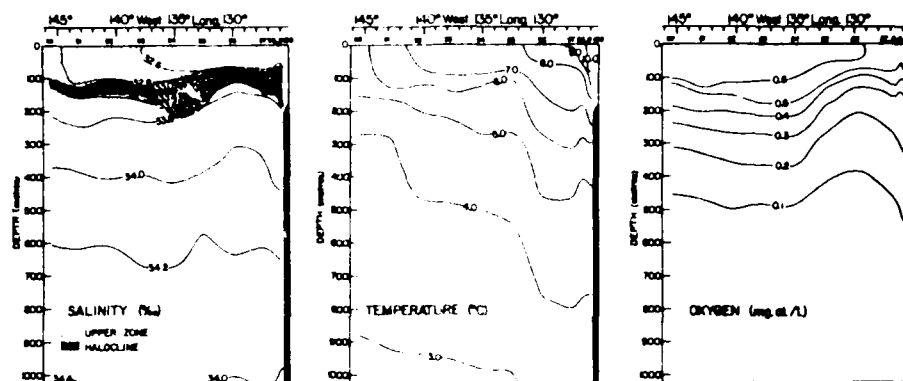


Figure 6d. Vertical sections of salinity, temperature, and dissolved oxygen along approximately latitude 49°N., winter 1958

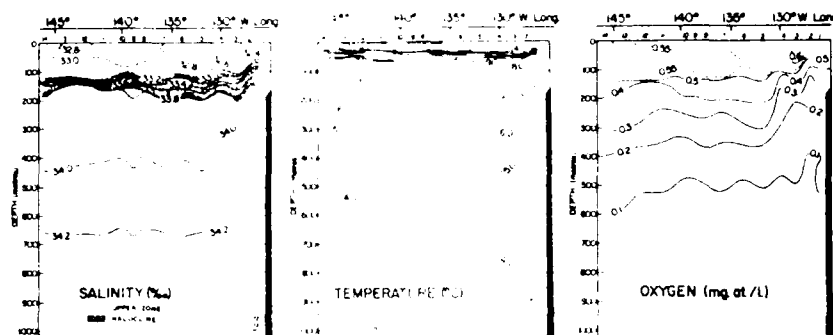


Figure 6e. Vertical sections of salinity, temperature, and dissolved oxygen along approximately latitude 48°N., summer 1959

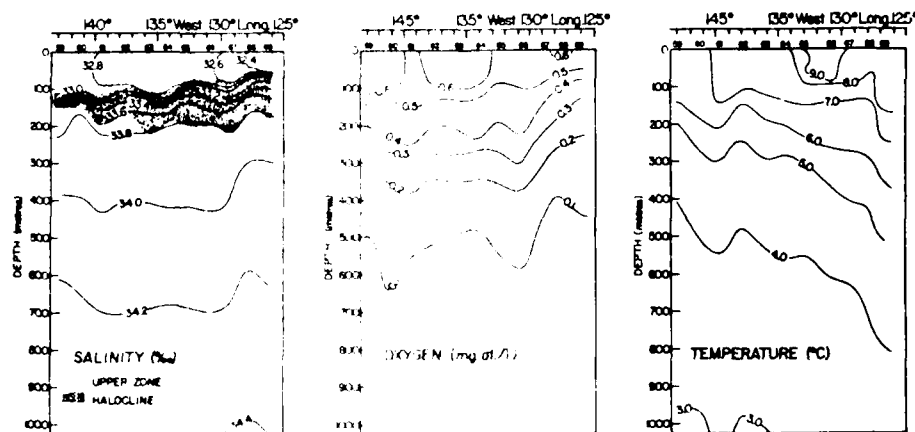


Figure 6f. Vertical sections of salinity, temperature, and dissolved oxygen along approximately latitude 47°N., winter 1959.

event, similar to that which took place in 1957, is going on at the present time (spring-summer 1983).

Seasonal changes in the thermal structure can be clearly seen by comparing Figure 6e with Figure 6f. The sharp, shallow thermocline in summer is missing in winter and the upper layer has cooled down from 14° to 8-9°C. Deeper down the thermal structure is largely unchanged with the 4°C isotherm being a bit steeper in the east in winter (Fig. 6f). Seasonal changes in salinity are less apparent. There is some suggestion that the halocline weakens and broadens slightly in winter.

Oxygen changes very little with season or position. The oxygen section along 49°N for the winter for 1958 (Fig. 6d) indicates the presence of upwelling off the shelf break in the possible form of a cyclonic eddy. This is consistent with the vertically coherent trough exhibited by the temperature section which could be the signature of a cold eddy. As will be discussed later cyclonic eddies are common features off this western Continental Shelf.

#### Sound velocity

Translated into sound velocities these temperature-salinity distributions result in a shallow (~100 m) salinity duct caused by a sound velocity minimum at this depth for all seasons (Fig. 7). In winter this minimum is less well isolated from the sea surface and extreme winter surface conditions can easily mix down to the minimum creating a surface duct. In the other seasons surface heating leads to a sharp increase in sound velocity corresponding to the strong, shallow seasonal thermoclines seen in Figure 6. The broad permanent sound channel, with its axis at about 400 m, is substantially deeper than the shallow duct at about 100 m. The



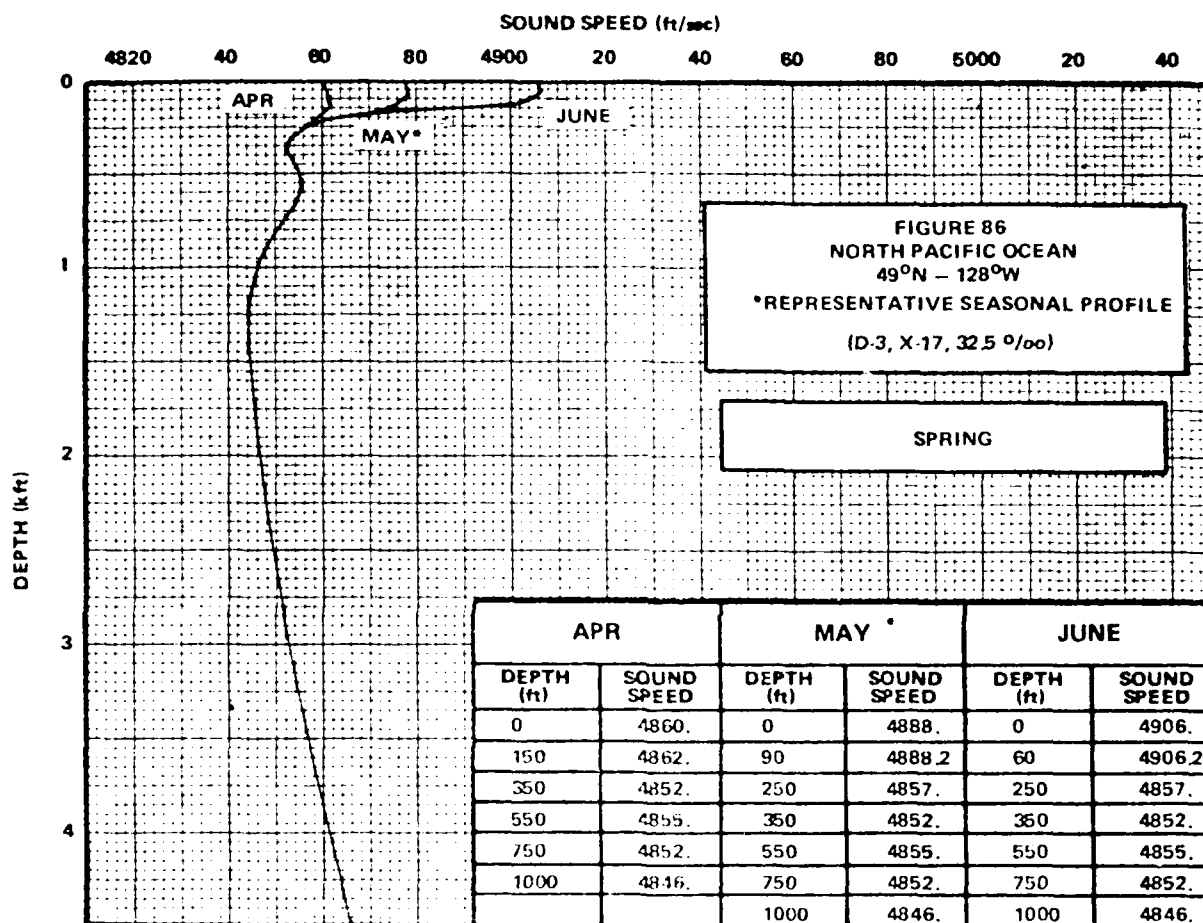


Fig. 7(a)

Figure 7. Seasonal sound velocity profiles off Juan de Fuca Strait

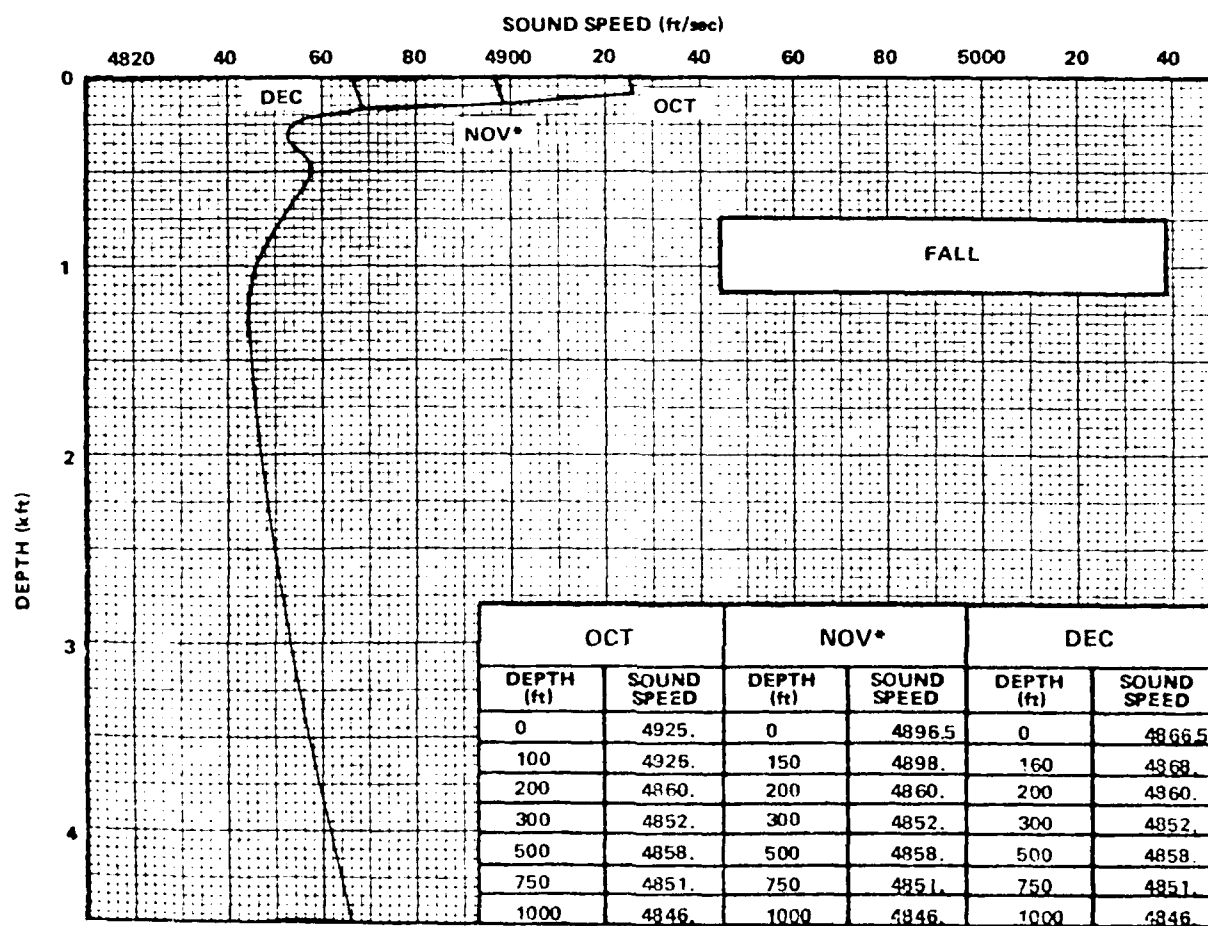


Fig. 7(b)

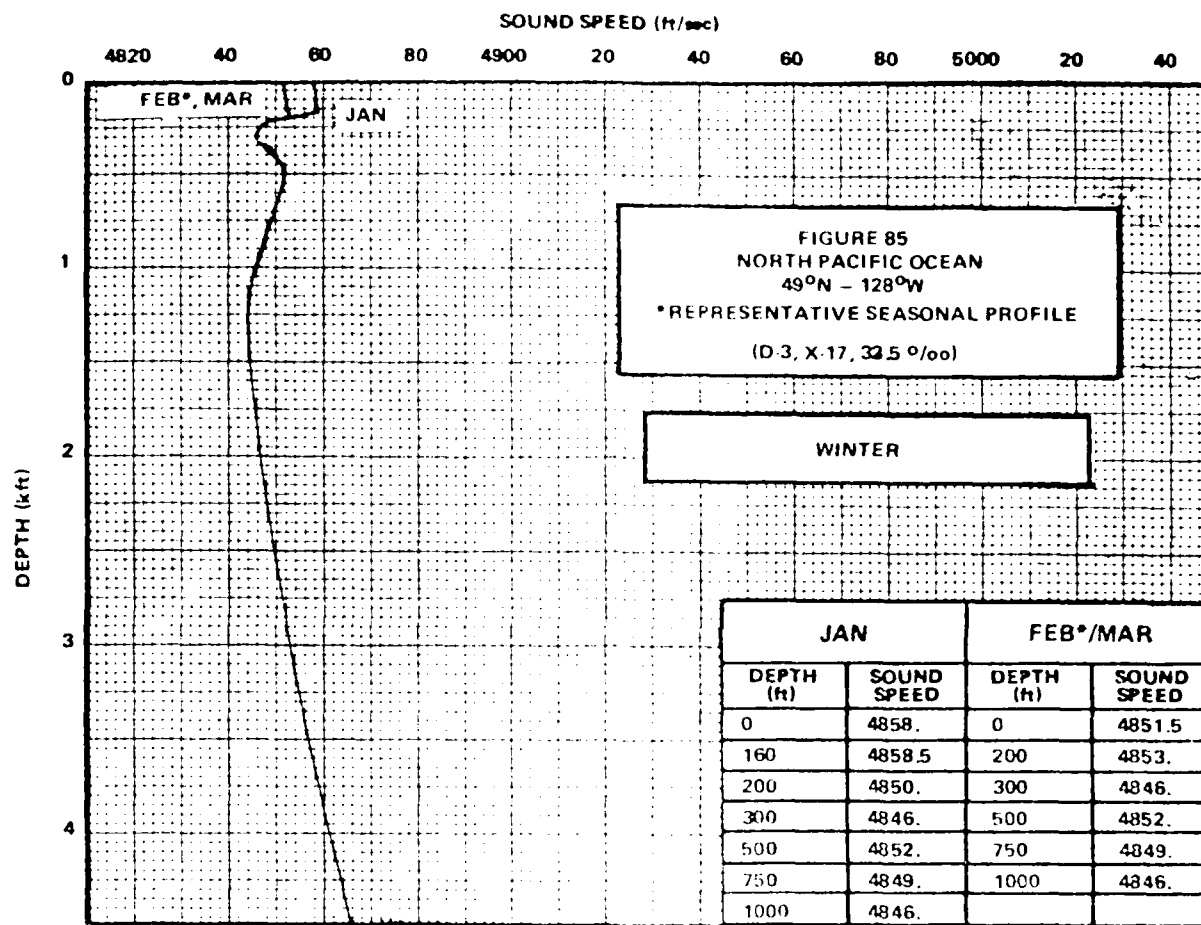


Fig. 7(c)

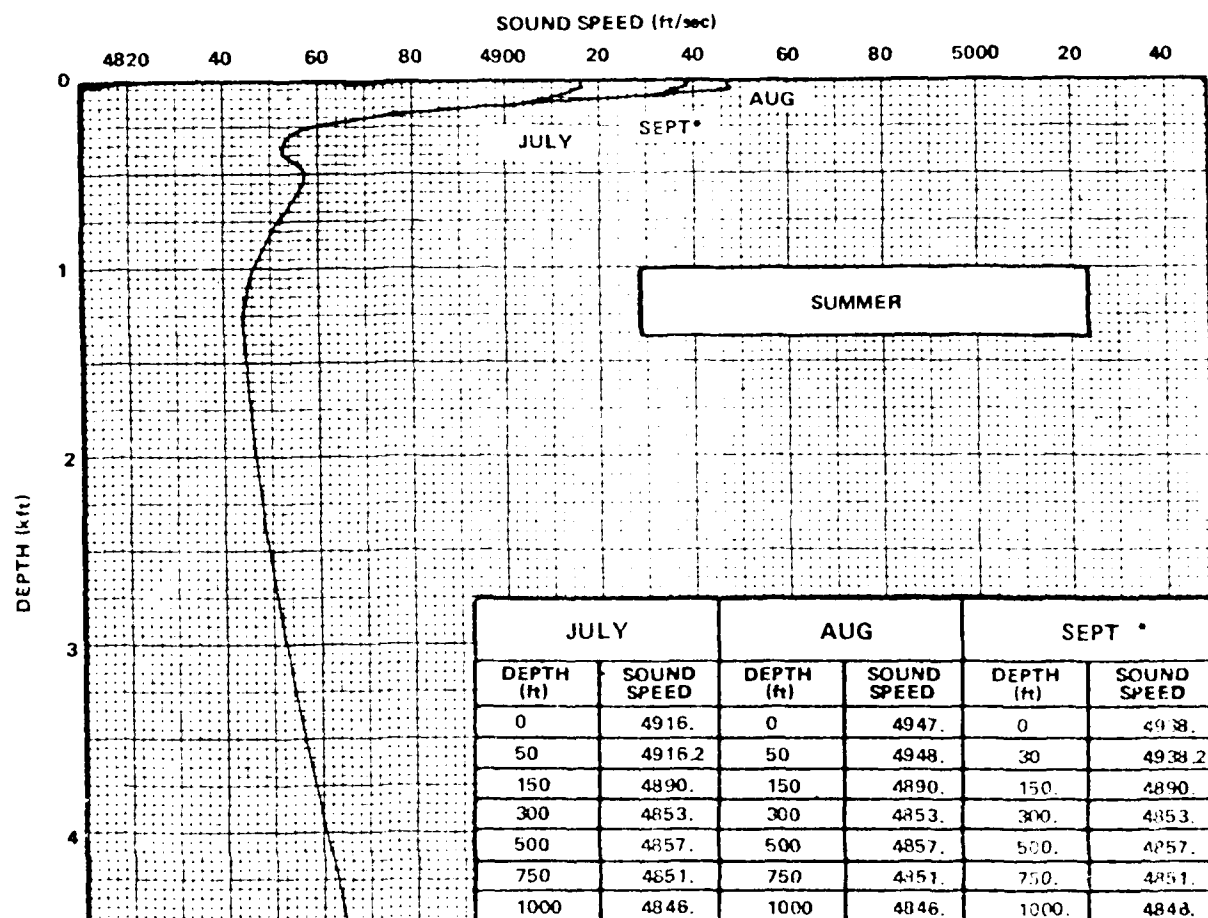


Fig. 7(d)

deeper sound velocity change corresponds to the permanent thermocline represented by the strongest vertical temperature gradients in the winter sections of Figures 6d and 6f.

To put the shallow duct into proper perspective the mean annual meridional sound velocity section, along 142.5°W, is shown as a family of 5° mean curves in Figure 7. Here the shallow duct can be clearly seen in the sound velocity profiles at 42°N and 57°N. South of 40°N this feature, which is related to the vertical salinity structure, is not usually observed. This shallow duct exists because the temperature profile either inverts (has a minimum) or is isothermal (flat) in a region where the salinity increases rapidly with depth. Thus it is the strong salinity gradient (halocline), at about 100 m, that coincides with the sound velocity minimum which forms the shallow duct. Farther to the west this feature is even more developed (Fig. 8) and the sound speed minimum is clearly marked in all the profiles north of 40°N.

The effects of secondary sound channels on acoustic propagation, in the Northeast Pacific, have been recently studied by Chow and Browning (1983). They demonstrate that high-frequency (~200 Hz) acoustic signals are effectively trapped in the duct leading to very long ranges in acoustic sensing and detecting. At lower frequencies (~35-50 Hz) acoustic energy leaks out of the shallow duct and into the deep sound channel (DSC). In their study the DSC axis was at about 400 m while the shallow duct was at 140 m not unlike conditions in our region of interest.

It is interesting to note the meridional development of the DSC with decreasing latitude in Figures 7 and 8. The easternmost section in Figure 7 indicates the DSC first emerging between 40 and 45°N in a profile clearly marked with a shallow



surface duct. The fact that the sound velocity, in our region of interest (47-49°N, 124-127°W), also contains a shallow duct and DSC merely reflects the fact that southern conditions extend slightly farther north along the coastal boundaries. As will be discussed with respect to the circulation, this probably varies with season.

### Vertical profiles

In order to better resolve some of the features discussed above it is instructive to consider a series of CTD data from September 1973 reported by Holbrook (1975). The station map for these casts is reproduced in Figure 9 with the specified region of interest added. The 100 and 500 m depth contours also clearly depict the pertinent bottom topography with the relatively wide Continental Shelf and the steep continental slope. The extension of Juan de Fuca Canyon up into Juan de Fuca Strait is also well depicted.

Looking at stations 56-63, going from deep water offshore up onto the shelf and into the canyon, we can see zonal changes of the water properties discussed above. The vertical profiles for temperature, salinity and density ( $\sigma_t$ ) are presented for each station in Figure 10. In general the same trends are seen as in the larger scale summer property sections of Figure 6. The summer thermocline runs from about 50 m offshore to about 30 m over the Continental Shelf (note the scale change on the depth axis). In the offshore stations (56-59) the permanent thermocline is located at about 200 m. The shelf stations do not go this deep. As with the previous sections the halocline (salinity gradient) is deeper than the summer thermocline particularly in the offshore stations.

It is interesting to note that in the offshore stations 57-60 there is a shallow (~100 m) temperature minimum which coincides with the halocline. As mentioned earlier it is this salinity gradient which produces a stable density structure (note the sigma-t curves) and allows the temperature inversion to persist. In many other ocean regions density is more strongly influenced by temperature alone and temperature minima can exist only for a short time before mixing eradicates them. In this series of profiles the temperature minimum is absent over the Continental Shelf where the shape of the salinity gradient (halocline) changes. Here the halocline is both stronger and shallower.

Another interesting difference between the offshore profiles and those over the shelf is the absence of fine-scale structure (small variations in T and s) in shallow water. In the deeper stations (i.e., Stns. 56, 57; Figs. 10a, 10b) fine structure is apparent in salinity both above and below the halocline, while temperature fine structure is most abundant in the thermal inversions. As will be discussed later this supports microstructure studies which identify the upper 200-m layer and the temperature inversions as sites of increased turbulence. In strong contrast the profiles from the Continental Shelf (i.e., Stns. 61, 63; Figs. 10g, 10h) exhibit no fine-scale structure in either temperature or salinity. This suggests that the region over the Continental Shelf is much less active in terms of turbulence and current shear than the region seaward of the shelf break. It will be shown later that all of the strongest mean flow and its variations occur over and offshore from the Continental Shelf break. Numerical model studies will use the shelf break as the onshore boundary.



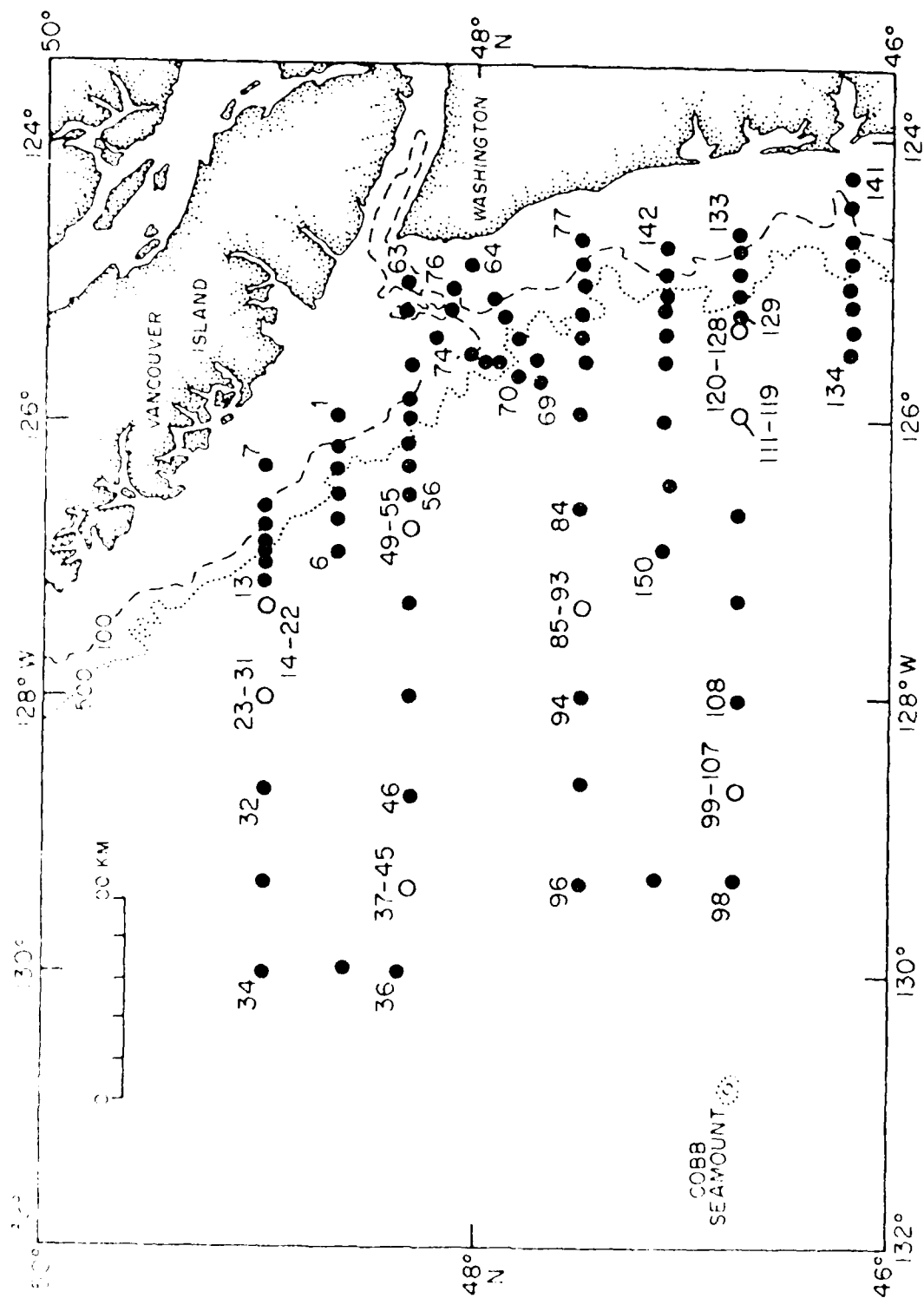
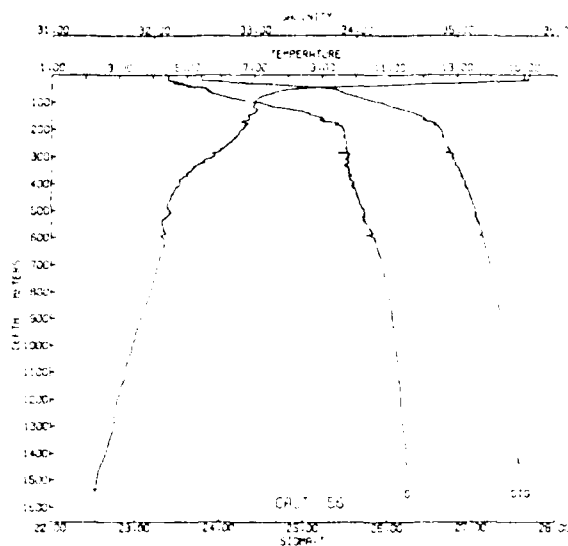
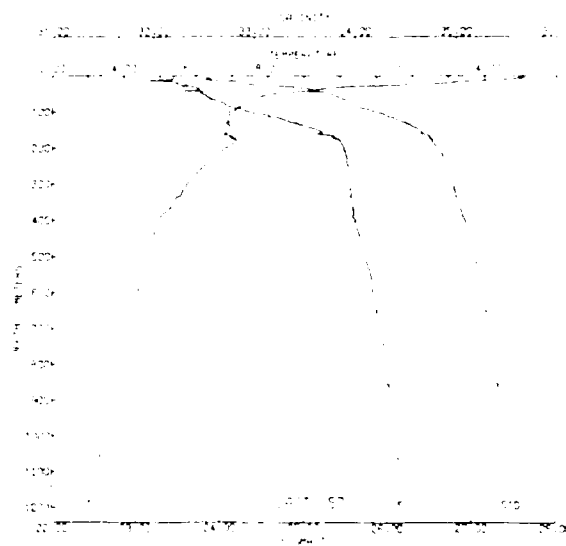


Figure 9. Location chart showing the STD station positions obtained during September 1973. ●'s identify single-cast stations and ○'s identify multicast stations.



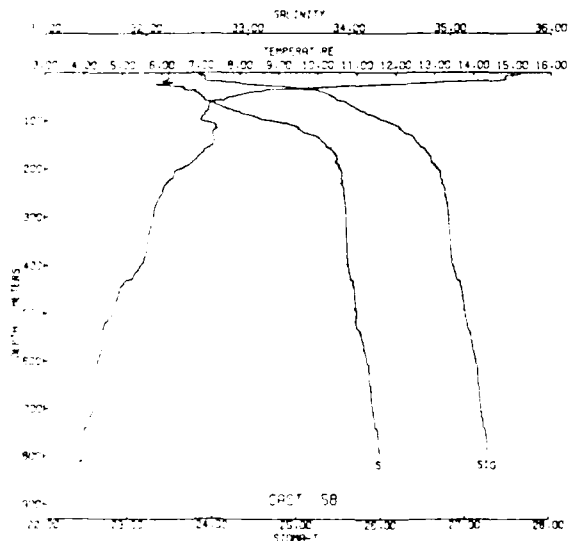
CAST HP-7-CC-356 DATE 13 SEP 73 TIME 1821 GMT  
 LAT 48 19.4N LONG 126 32.5W WEATHER 1 SEA STATE 2  
 BAROMETER 15 WIND DIR 332 T SPD 06 KT VISIBILITY 7  
 CLOUD 6 AMOUNT 0 DRY 15.3 WET 13.1 DEPTH 1616 M

Fig. 10(a)



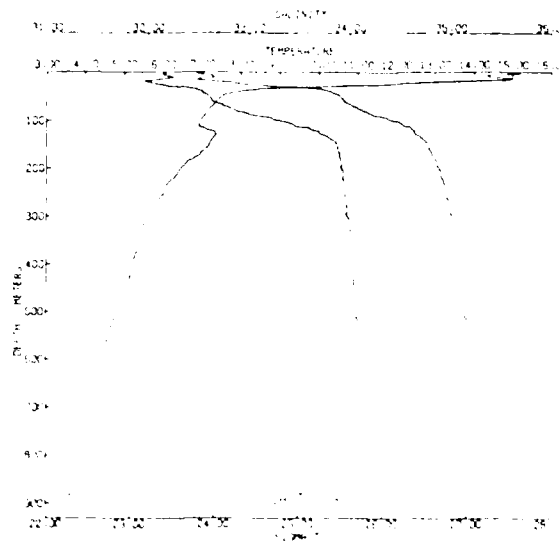
CAST HP-7-CC-357 DATE 13 SEP 73 TIME 2003 GMT  
 LAT 48 11.7N LONG 126 21.0W WEATHER 1 SEA STATE 2  
 BAROMETER 15 WIND DIR 350 T SPD 03 KT VISIBILITY 7  
 CLOUD 0 AMOUNT 2 DRY 16.8 WET 13.8 DEPTH 1174 M

Fig. 10(b)



CAST HP-7-CC-359 DATE 13 SEP 73 TIME 2254 GMT  
 LAT 48 19.7N LONG 126 30.4W WEATHER 1 SEA STATE 2  
 BAROMETER 15 WIND DIR 321 T SPD 04 KT VISIBILITY 7  
 CLOUD 5 AMOUNT 2 DRY 16.0 WET 13.4 DEPTH 3576 M

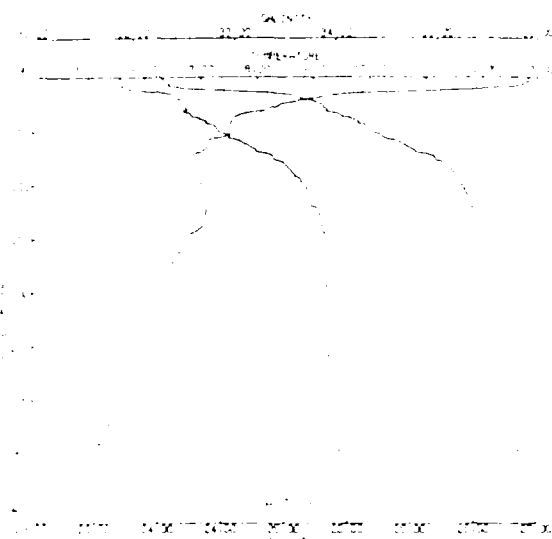
Fig. 10(c)



CAST HP-7-CC-058 DATE 13 SEP 73 TIME 2138 GMT  
 LAT 48 20.2N LONG 126 11.3W WEATHER 1 SEA STATE 2  
 BAROMETER 15 WIND DIR 340 T SPD 05 KT VISIBILITY 7  
 CLOUD 0 AMOUNT 2 DRY 16.5 WET 13.2 DEPTH 0805 M

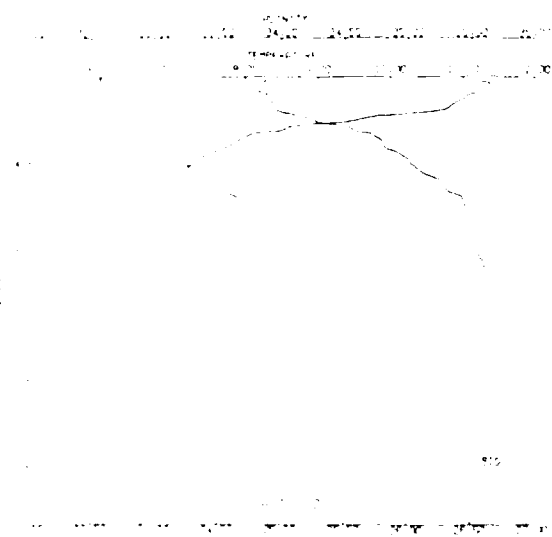
Fig. 10(d)

Figure 10. CTD profiles off Juan de Fuca Strait (positions as in Figure 9)



LAST WP-7-CC-60 DATE 14 SEP 73 TIME 0100 GMT  
LAT 43 13.0N LONG 125 52.5W WEATHER 1 SEA STATE 2  
WIND 15 KNOTS WIND DIR 304 T CLOUD 0 VISIBILITY 7  
CLOUD 0 AMOUNT 0 DRY 10.1 WET 14.0 DEPTH 308 M

Fig. 10(e)



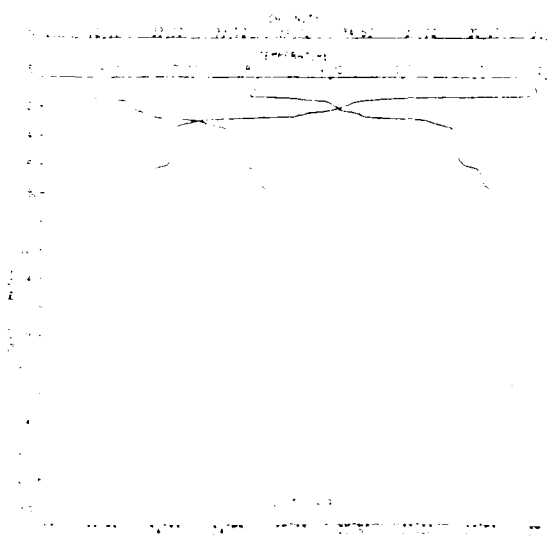
LAST WP-7-CC-61 DATE 14 SEP 73 TIME 0230 GMT  
LAT 43 13.3N LONG 125 37.0W WEATHER 1 SEA STATE 2  
WIND 15 KNOTS WIND DIR 335 T CLOUD 0 VISIBILITY 7  
CLOUD 0 AMOUNT 0 DRY 10.1 WET 13.5 DEPTH 3214 M

Fig. 10(g)



LAST WP-7-CC-61 DATE 14 SEP 73 TIME 0126 GMT  
LAT 43 13.3N LONG 125 37.0W WEATHER 1 SEA STATE 2  
WIND 15 KNOTS WIND DIR 335 T CLOUD 0 VISIBILITY 7  
CLOUD 0 AMOUNT 0 DRY 10.1 WET 13.5 DEPTH 3214 M

Fig. 10(f)



LAST WP-7-CC-61 DATE 14 SEP 73 TIME 0230 GMT  
LAT 43 13.3N LONG 125 37.0W WEATHER 1 SEA STATE 2  
WIND 15 KNOTS WIND DIR 335 T CLOUD 0 VISIBILITY 7  
CLOUD 0 AMOUNT 0 DRY 10.1 WET 13.5 DEPTH 3214 M

Fig. 10(h)

### Stability Profiles (Brunt-Vaisälä Frequency)

Translated into Brunt-Väisälä frequency (BVF) profiles (Fig. 11) the 5° square mean temperature and salinity profiles reveal a region dominated by a high stability frequency gradient at about 100 m. There is a small subsurface maximum at around 500 m much like the neighboring BVF profiles. These features can be seen a bit more clearly in the log. BVF (log N) versus depth profiles from individual May 1980 CTD casts (Fig. 12). As discussed in Lueck et al. (1983) these profiles break naturally into three depth ranges. In the upper 25-100 m BVF values (N values) are widely scattered reflecting the varying inputs of surface heating, evaporation, and fresh water inflow. Large turbulent dissipations were observed in this range. Temperature inversions (primarily minima) were also prevalent over this depth range.

The water column between 100 and 200 m contains a strong gradient in BVF and data from the various coastal CTD stations appear similar. Over this range turbulence decreases in response to the stronger gradients. Below 200 the BVF decreases exponentially with depth. Observed turbulence was very low beneath this depth with dissipation levels the lowest ever reported (Lueck et al., 1983).

The mean BVF profile (Fig. 11), off the mouth of Juan de Fuca Strait, yielded an internal Rossby radius of 16.6 km. This represents the length scale (multiply by 2 ) of circulation features (meanders, eddies, etc.) which are in geostrophic balance (can be described using dynamic height, thus depend primarily on the density structure). Thus feature lengths should be about 100-200 km which will be shown later to be the wavelength of the optimally growing baroclinic wave predicted by linear theory. In other words, dynamical theory which includes the local stratifica-

tion (vertical density structure) predicts the growth of a 100-m wave taking energy from the mean flow.

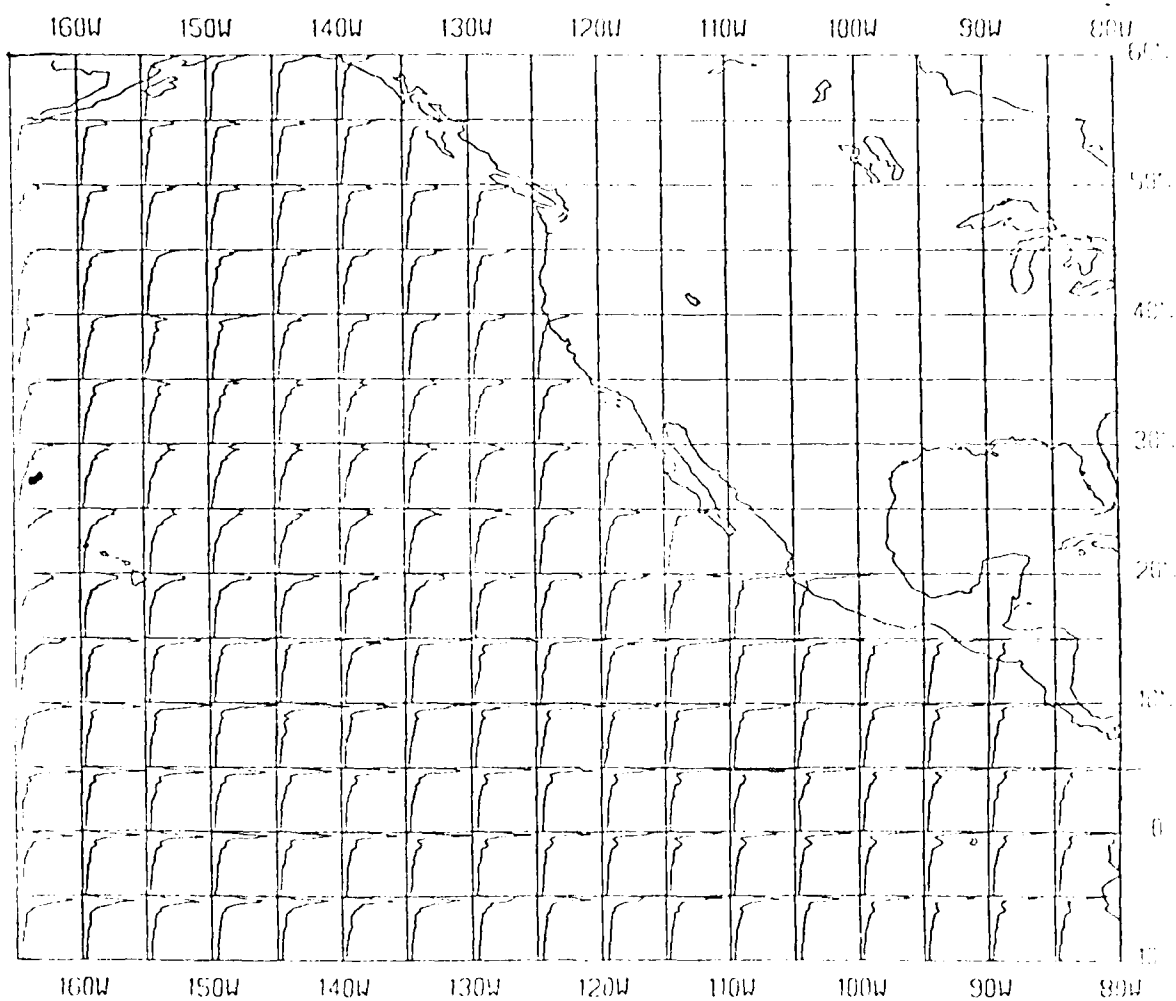
## Circulation

### Seasonal and Annual Mean Currents

There are many different descriptions of the general circulation pattern in the eastern North Pacific. A useful schematic representation, produced by Roden (1975), is presented here as Figure 13. It depicts the flow as a large cyclonic gyre in the Gulf of Alaska. A similar schematic (Fig. 14), taken from an earlier paper by Dodimead et al. (1963), gives more definition to this gyre showing it as a "pear-shaped" feature concentrated in the western Gulf of Alaska. This suggests that flow along the eastern boundary (our region of interest) is weaker and less coupled to the main gyre. It should also be noted that in this scheme (Fig. 14) the surface flow direction in our area is southward marking the start of the California Current. This represents summer conditions predominantly sampled by the various observational program. In contrast surface flow in winter is northward marking a southward shift of the cyclonic gyre. This separation of flow, at the eastern end of the west-wind drift/subarctic current combination (now usually referred to as the North Pacific Current), into north and south components has both seasonal and year-to-year changes.

These changes are best demonstrated with a sequence of dynamic topography charts for the sea surface relative to 1000 db (or m). These charts (Fig. 15) were published by Dodimead et al. (1963). It should be remembered that the period

# PACIFIC FIVE DEGREE SQUARES



Brunt-Väisälä frequency ( $N$  in  $10^{-3} \text{ s}^{-1}$ ) profiles for the North Pacific.

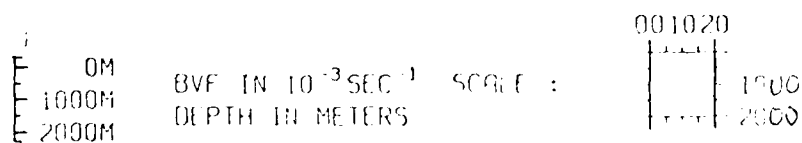


Figure 11. Brunt-Väisälä frequency profiles (0-2000 m) by 5° square in the eastern North Pacific

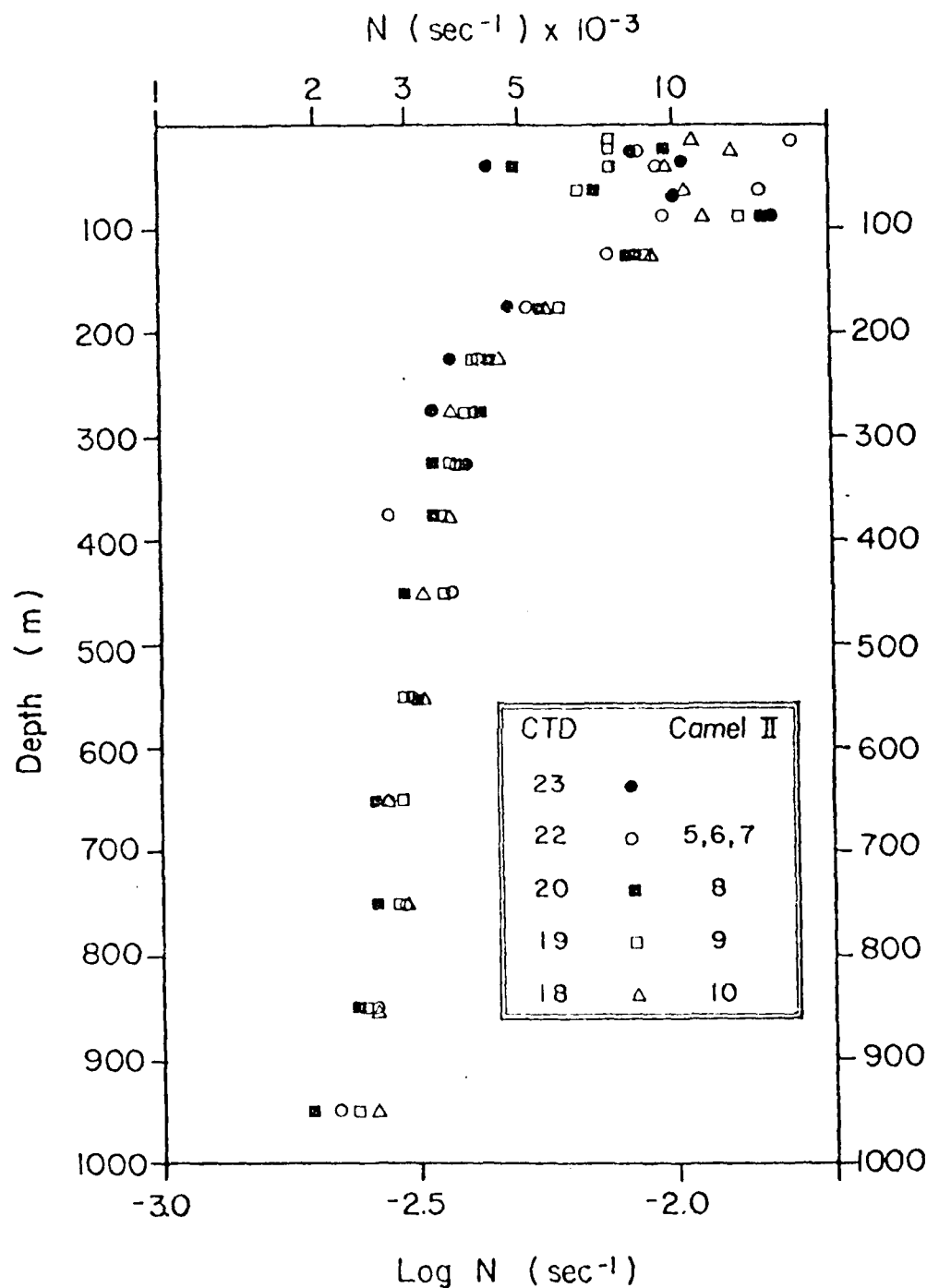


Figure 12. Log profiles of Brunt-Väisälä frequency ( $N$ ) from individual CTD profiles off Juan de Fuca Strait

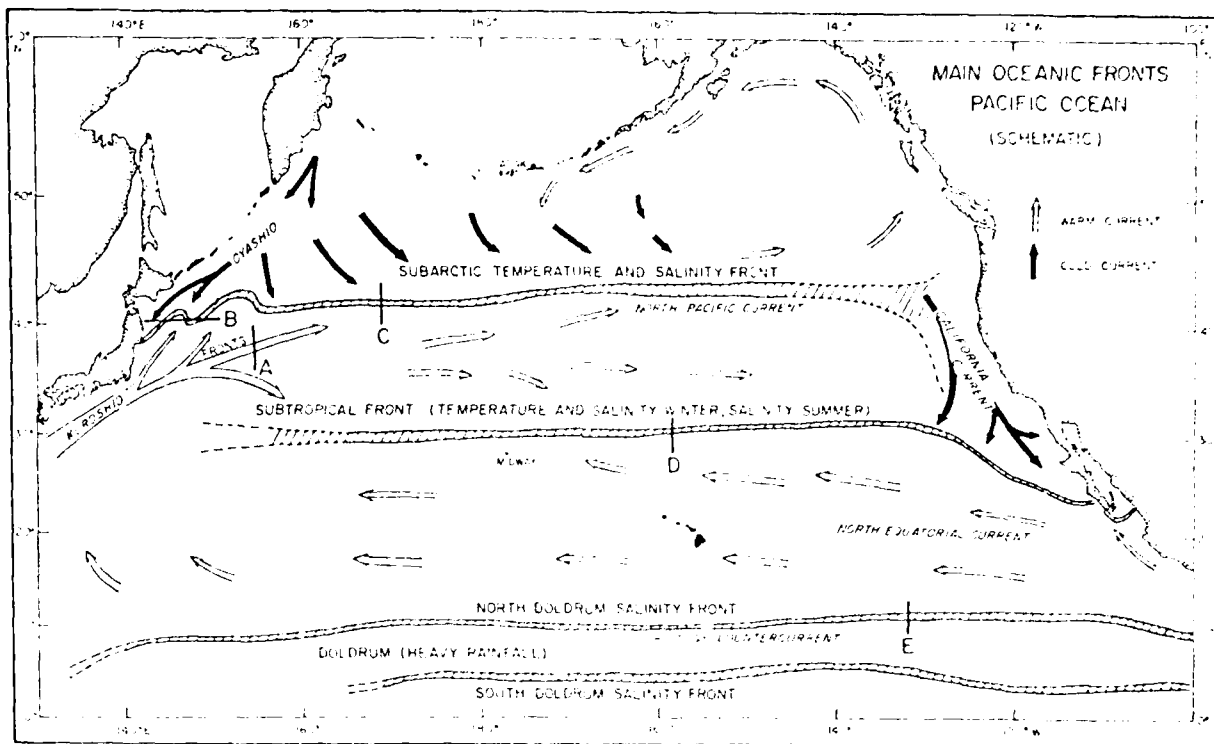


Figure 13. Schematic map of main North Pacific fronts. Arrows indicate prevailing current directions. Letters refer to fronts A, Kuroshio front; B, Oyashio front; C, subarctic front; D, subtropical front; E, doldrum front

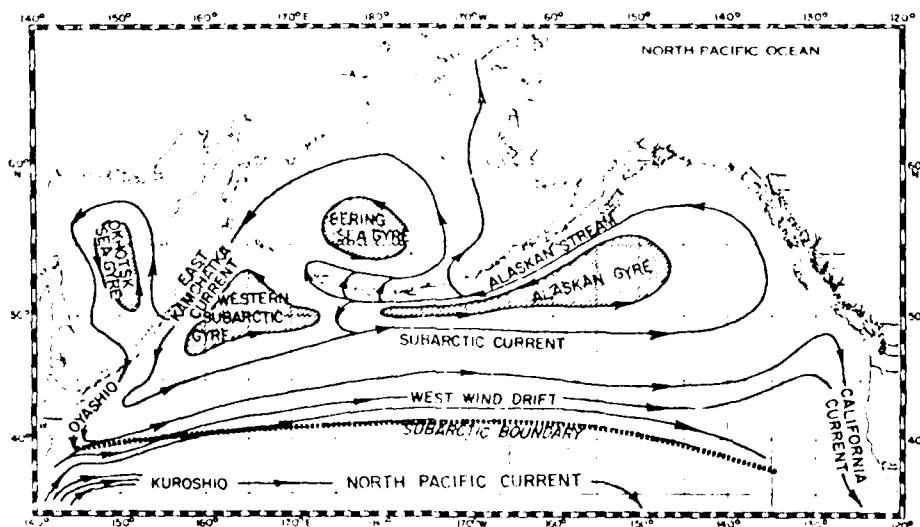


Figure 14. Schematic diagram of surface circulation relative to 1000 decibars



covered, especially the years 1957-58, represented anomalous conditions in coastal sea surface temperature and sea level (Tully et al., 1960).

The most complete map is for the summer of 1955 (Fig. 15a). Conditions for this year are likely to be typical and the flow patterns considered representative, at least on the large scale. In this map flow directions are indicated by small arrow-heads and the strength of the flow is inversely proportional to the distance between contour lines as indicated in the speed nomogram. The summer shows the splitting of the eastward flowing current into northward and southward segments at about  $45^{\circ}\text{N}$ ,  $145^{\circ}\text{W}$ . This is just south and west of the candidate study region. Note how not all of the flow, in the westward Alaskan stream, appears to recirculate in the west.

In the summer of 1956 (Fig. 15b) this stream appears more continuous to the west. The north-south current split has moved east to  $45^{\circ}\text{N}$ ,  $135^{\circ}\text{W}$ . In both years the summer surface flow in our region is southward starting somewhere along Vancouver Island and continuing on down the coast.

This whole pattern shifts somewhat to the south in the winter of 1957 (Fig. 15c) bringing northward flow to most of the region. The unusual conditions of 1957 produce a very strange flow pattern for the summer of 1957 (Fig. 15d). The north-south current split takes place farther west ( $\sim 145^{\circ}\text{W}$ ) with the isolines turning farther south. This creates a stagnation point (flow will not go north or south) just off the mouth of Juan de Fuca Strait.

By the winter of 1958 (Fig. 15e) the flow, off the Strait, is once again northward feeding into a strong coastal flow. This is consistent with the suspected stronger northward coastal flow in the anomaly years. In 1983 two satellite-tracked

drifting buoys moved rapidly northward along the west coast (Fig. 16). One buoy travelled from San Francisco to Cape Flattery (mouth of Juan de Fuca Strait) where it was picked up. During this transit it achieved daily speeds of up to 100 cm/sec travelling about 5 km offshore. A buoy farther north (Fig. 16) turned up into the Gulf of Alaska also travelling at speeds in excess of 100 cm/sec before running aground on Kodiak Island.

Figure 15f, from the summer of 1958, shows a return to southward flow along the coast of Vancouver Island and through our area of interest. This is due to a much sharper northward turn of eastward flow at about  $150^{\circ}\text{W}$  than was seen in the summer of 1957. The subsequent winter (Fig. 15g) brings a return of northward flow shifting back to southward current in summer (Fig. 15h).

A better overview of the seasonal shift can be gained by looking at the climatological mean (computed from all available data) dynamic topographies compiled by Wyrski (1974). The annual average surface, relative to 1000 db, (Fig. 17) indicates that the current split is located at our region of interest ( $\sim 48^{\circ}\text{N}$ ). Thus the mean position of the north-south shift is just off the mouth of Juan de Fuca Strait.

The first seasonal map covers the months of January and February (Fig. 18a) and likewise indicates the current split at our latitude of interest. Relative to the annual mean, however, the pattern appears to have shifted slightly south (typical winter shift) bringing northward flow closer to the coast of Vancouver Island. The March-April map (Fig. 18b) is very much like the previous period. The beginning of a shift back north can be seen in Figure 18c (May-June) where the 130 dyn cm line turns back to the north. This northward progression continues in July-August (Fig. 18d) bringing southward flow farther up the west coast. By September and October

[illegible]

**Figure 16. Satellite tracked buoy trajectories. Eastern and northernmost tracks consist of daily average positions.**

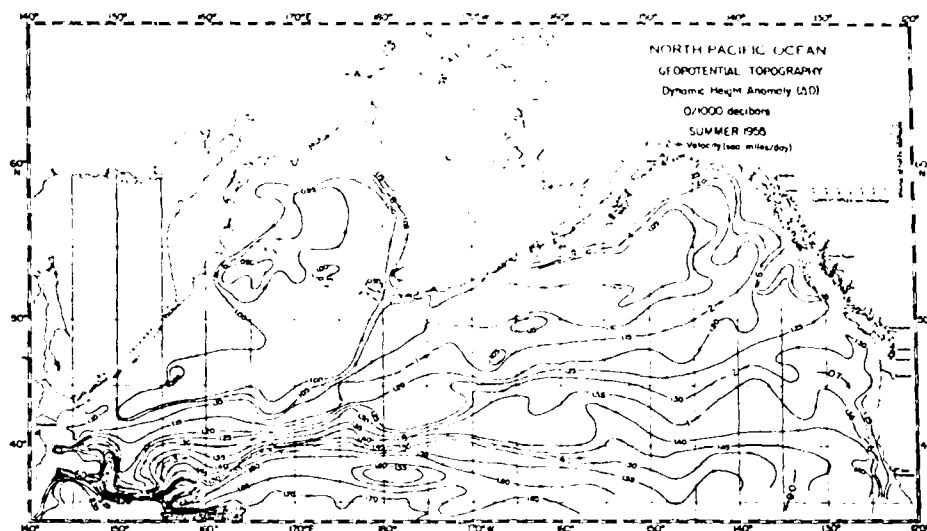


Figure 15a. Geopotential topography, 0/1000 decibars, summer 1955

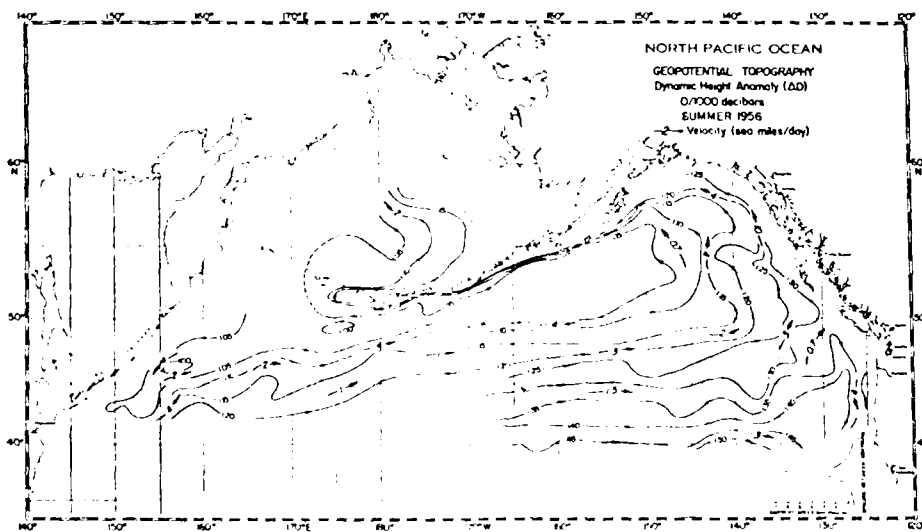


Figure 15b. Geopotential topography, 0/1000 decibars, summer 1956

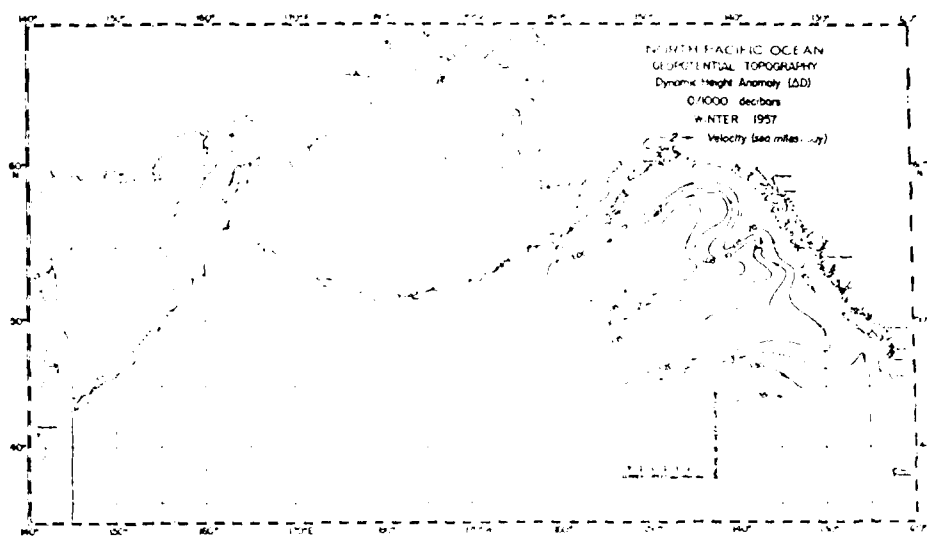


Figure 15c. Geopotential topography, 0/1000 decibars, winter 1957

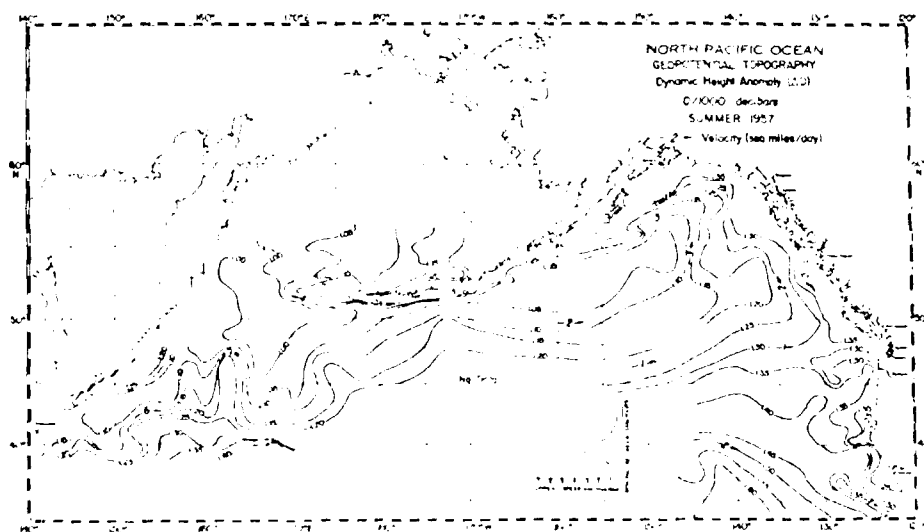


Figure 15d. Geopotential topography, 0/1000 decibars, summer 1957.

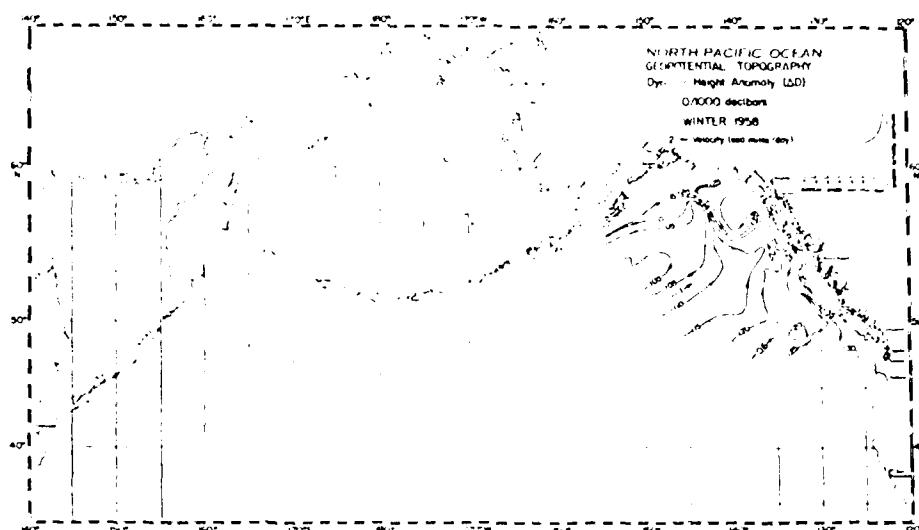


Figure 15e. Geopotential topography, 0/1000 decibars, winter 1958

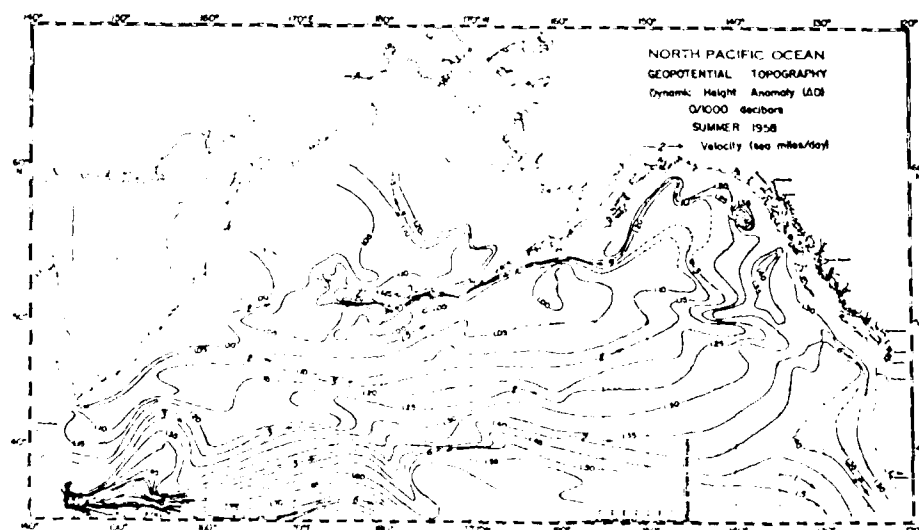


Figure 15f. Geopotential topography, 0/1000 decibars, summer 1958

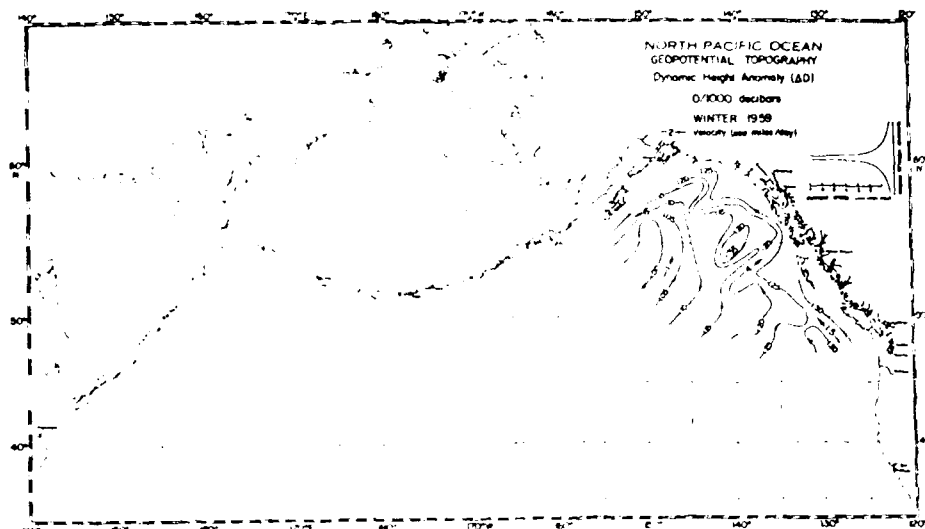


Figure 15g. Geopotential topography, 0/1000 decibars, winter 1959

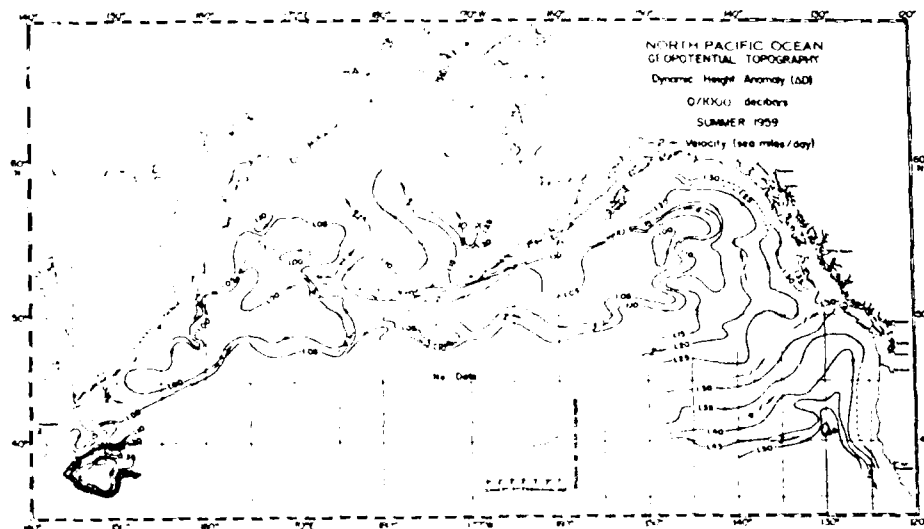


Figure 15h. Geopotential topography, 0/1000 decibars, summer 1959

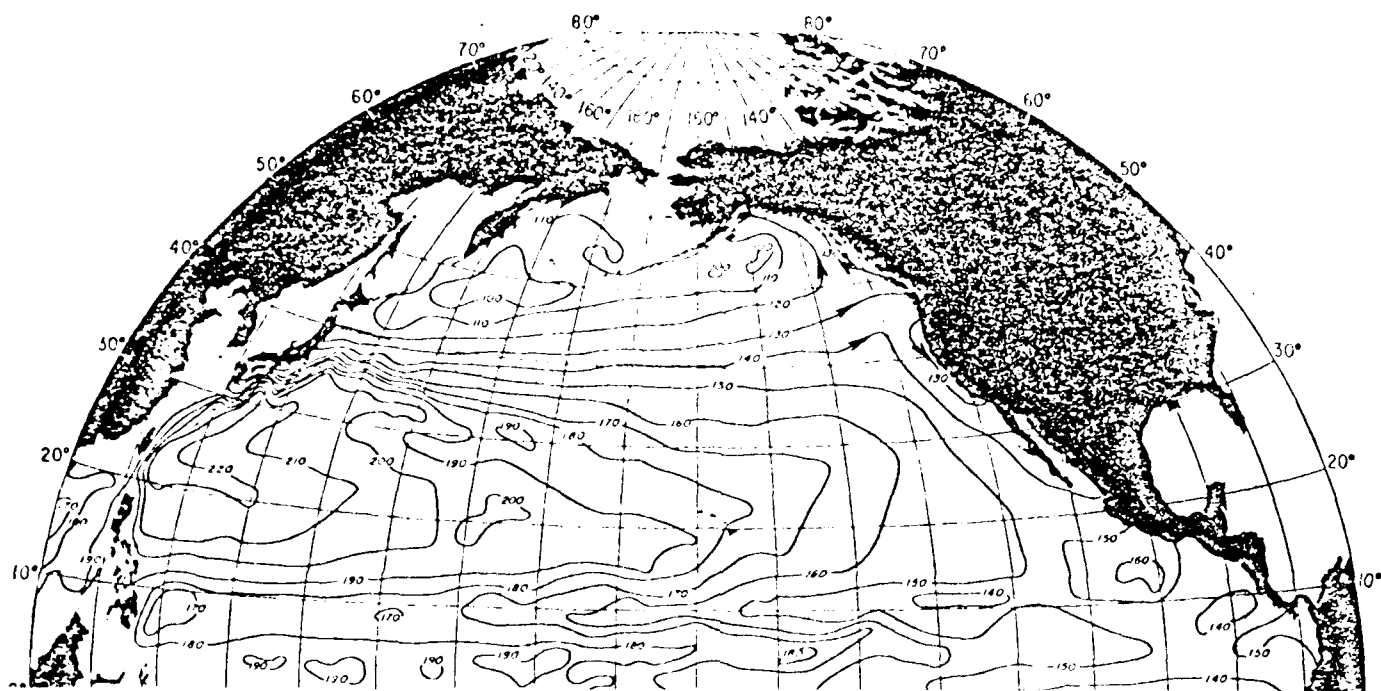


Figure 17. Mean annual dynamic topography of the sea surface relative to 1000 db in dyn cm; 36,356 observations



(Fig. 18e) and further into November-December (Fig. 18f) the southward flow moves both north and east to flow along the west coasts of Vancouver Island and Washington State. The winter southward migration of northward cyclonic flow does not begin until January-February (Fig. 18a).

To this seasonal variation of the near surface current must be added the marked annual change in the California Undercurrent which extends northward into the area of interest. As reviewed by Hickey (1979), the California Undercurrent is a vertical maximum in northward flow usually located below the main pycnocline (maximum density gradient) and seaward of the Continental Shelf. North of Pt. Conception, California, this undercurrent is strongest in winter during which time it often reaches to the surface to join with the northward flowing surface current (often called the Davidson Current).

This undercurrent is often described as a jet and has been observed to be quite narrow as depicted in Figure 19. Here the undercurrent's proximity to the continental slope is quite apparent. As will be shown later this undercurrent meanders off of the slope in conjunction with surface current meanders and eddy formation. In the region of interest current meter measurements (Thomson and Crawford, 1982; Freeland and Denman, 1982) have indicated that the undercurrent is symmetrical with respect to the offshore axis. The vertical current structure is also very narrow leading to the identification of this current as a jet.

The core of the undercurrent is characterized by high temperature, salinity and phosphate, and low dissolved oxygen as it carries water of equatorial origin as far northward as Vancouver Island. In our region of interest salinity of the undercurrent is about 33.9‰ while the temperature is about 7.0°C. The actual percent

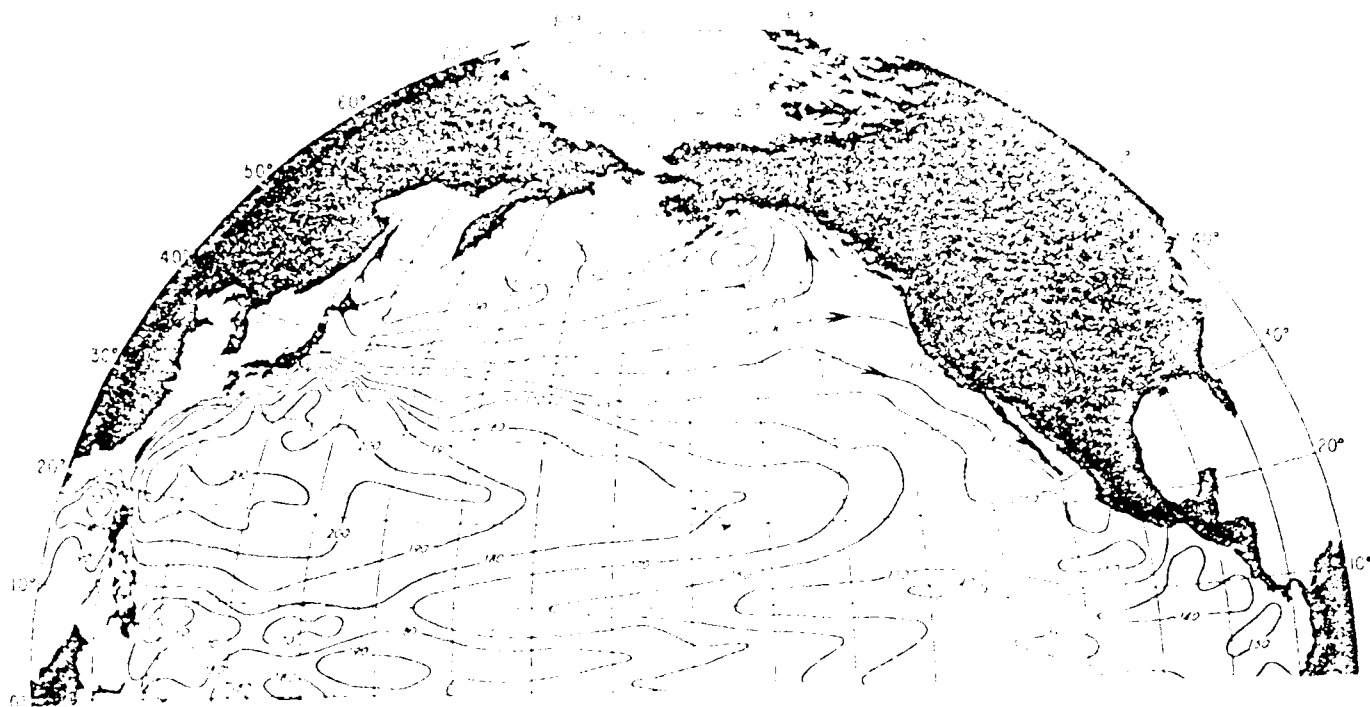


Figure 18a. Mean dynamic topography of the sea surface relative to 1090 db in dyn cm for the period January-February; 5506 observations.

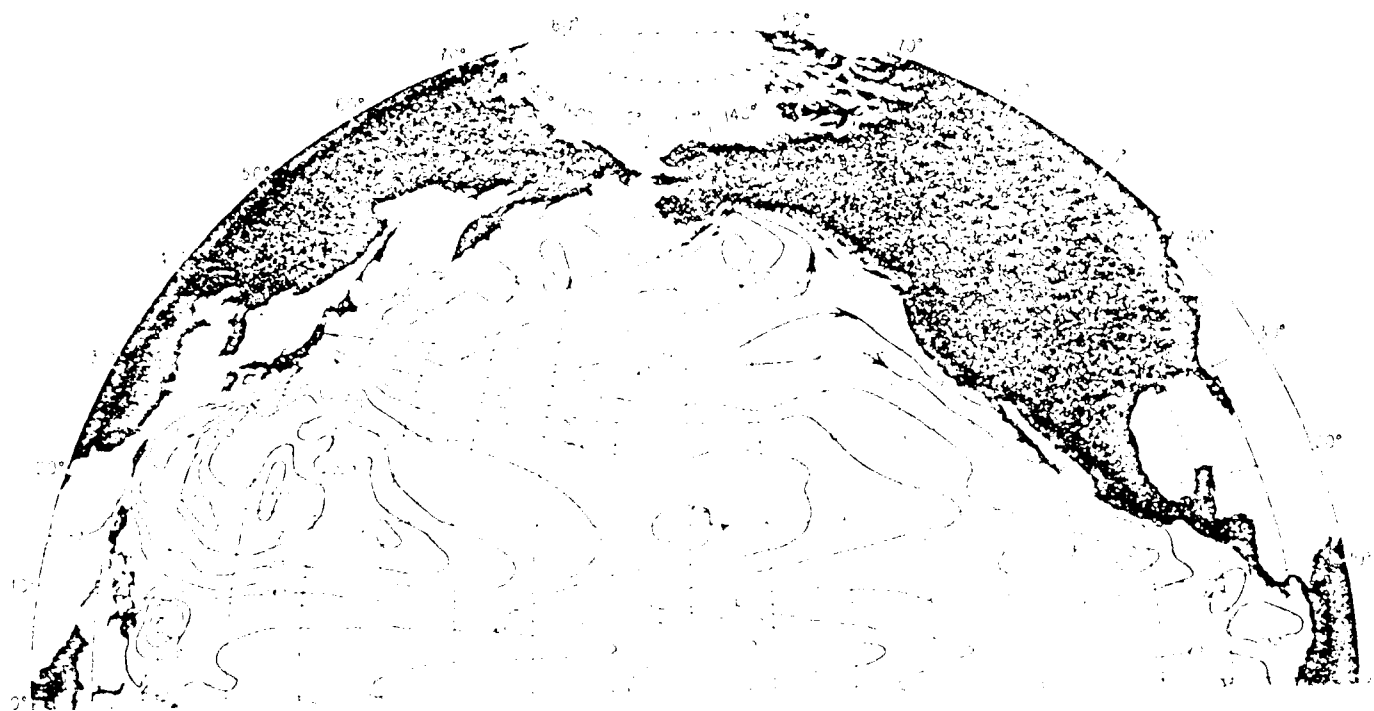


Figure 18b. Mean dynamic topography of the sea surface relative to 1090 db in dyn cm for the period March-April; 571 observations.

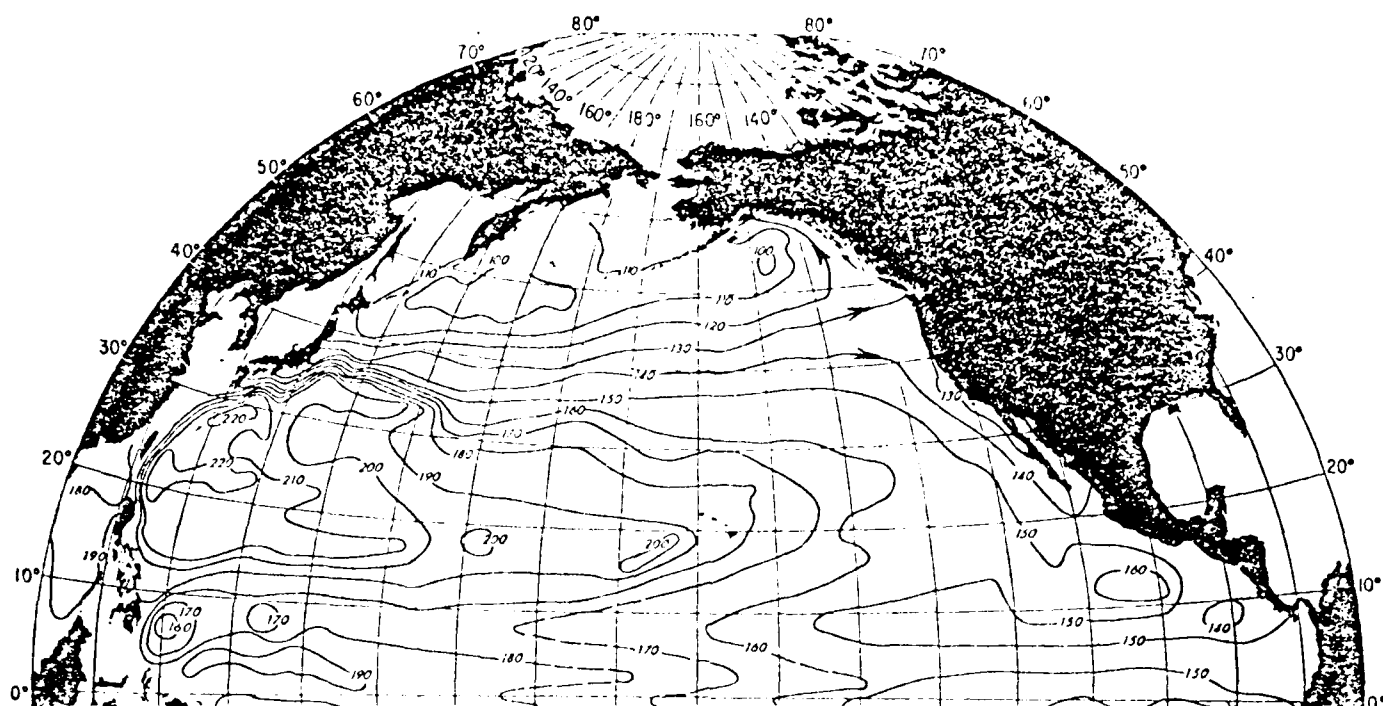


Figure 18c. Mean dynamic topography of the sea surface relative to 1000 db in dyn cm for the period May-June; 6609 observations

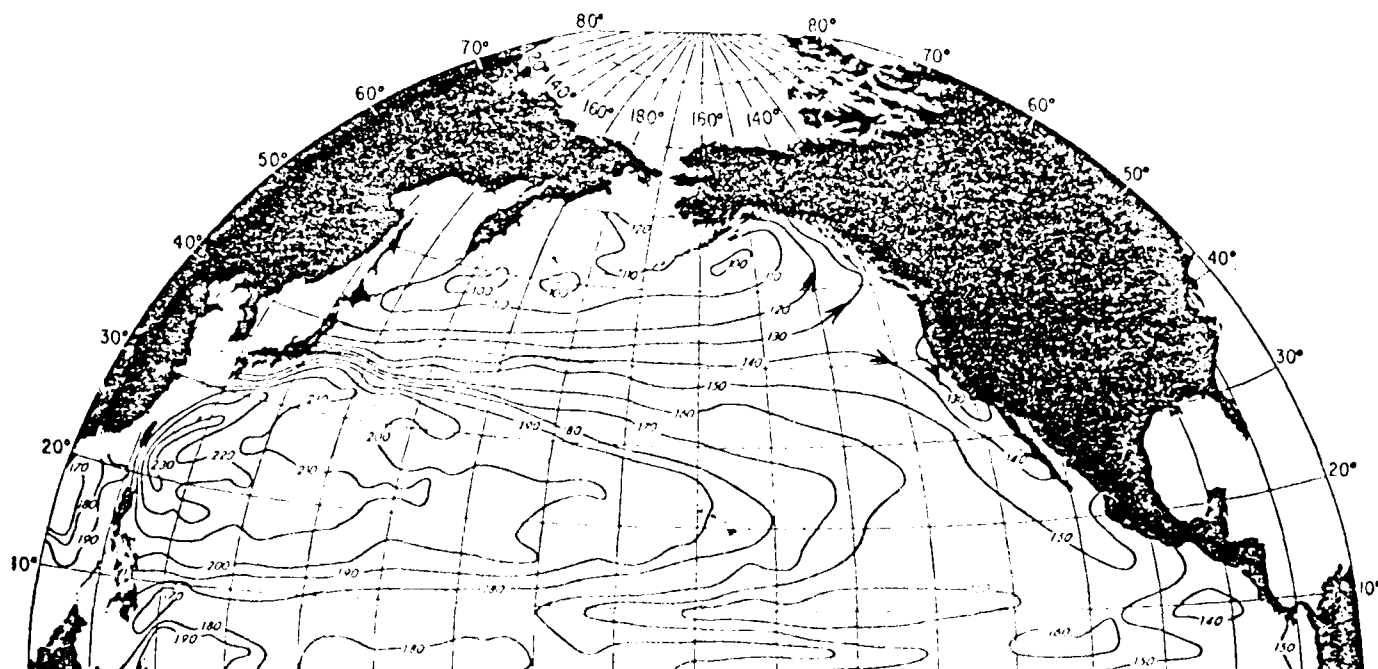


Figure 18d. Mean dynamic topography of the sea surface relative to 1000 db in dyn cm for the period July-August; 9196 observations

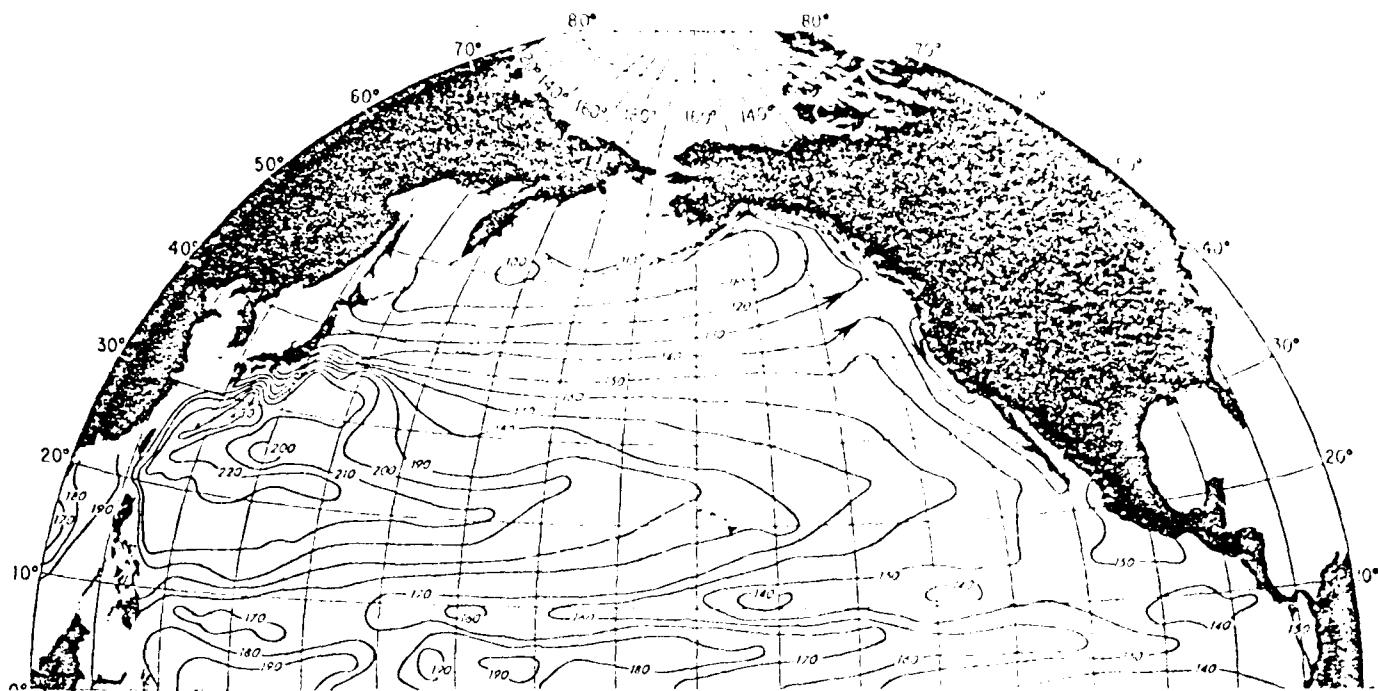


Figure 18e. Mean dynamic topography of the sea surface relative to 1000 db in dyn cm for the period September-October; 5243 observations

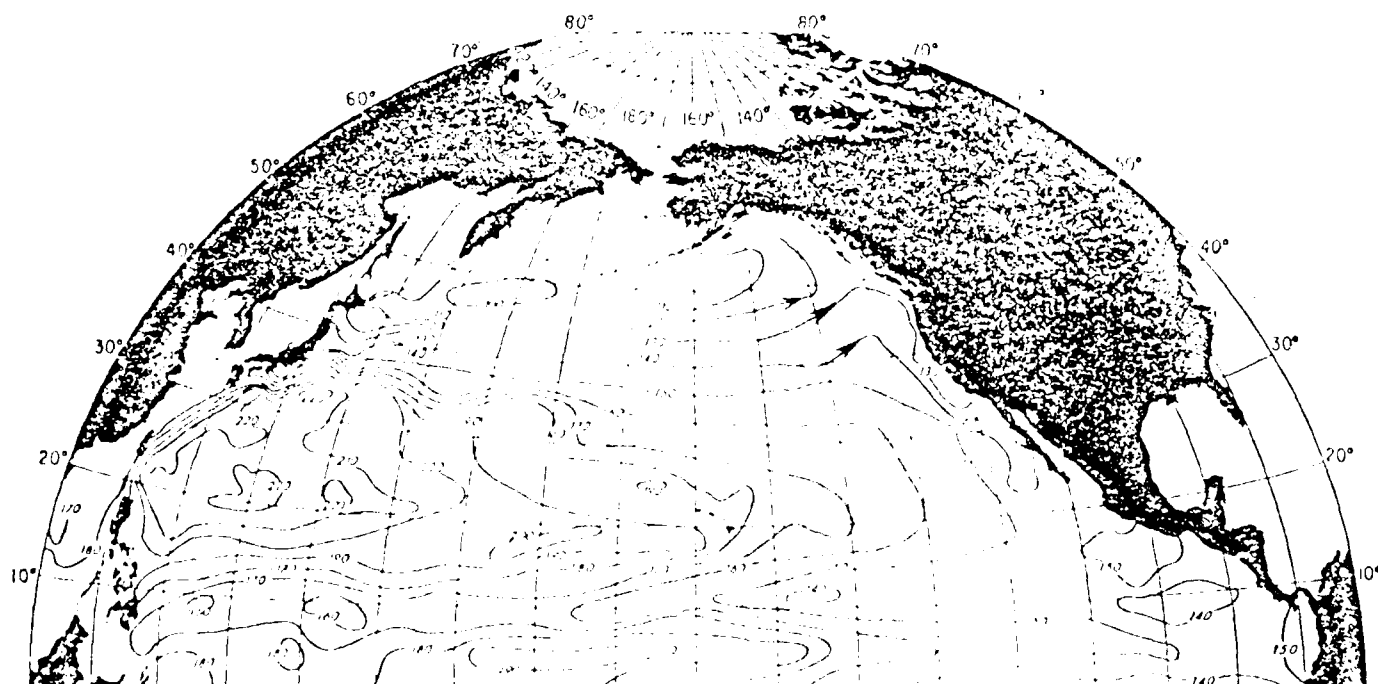


Figure 18f. Mean dynamic topography of the sea surface relative to 1000 db in dyn cm for the period November-December; 1060 observations

of equatorial water present in the undercurrent off Juan de Fuca Strait has not been determined.

As mentioned above the California Undercurrent (CUC) is strongest in the study region in winter when it extends to the surface to join the northward flowing surface, or Davidson, current. In spring the CUC weakens while the surface current shifts from northward to southward (see preceeding discussion of mean currents). Thus in spring the entire upper layer (0-500 m) flows to the south, and the CUC is absent. In summer while the surface current continues to flow to the south the CUC strengthens to again extend northward into our study area. This presence of strong vertical current shear extends into the fall.

In summary, the mean currents off the Strait of Juan de Fuca can be described as varying over three distinct seasons. In spring both the surface and deeper layers flow southward (no CUC). Sometime in early summer (May-June) the CUC extends into the region flow north under the southward surface current. The undercurrent continues to strengthen over the summer and fall. Thus summer and fall can be considered as single season characterized by strong vertical shear with surface flow to the south and an undercurrent flowing northward. In winter the surface current reverses to flow north in conjunction with the deeper northward undercurrent.

Many of these features can be clearly seen in almost two-year-long current meter records from a line of four moorings just north of Juan de Fuca Canyon (Fig. 3). These time series were presented by Freeland and Denman (1982) and are reproduced here as Figure 20. Also included, at the top of the diagram, is an upwelling index which primarily reports on the strength of the alongshore wind; positive for northerly (southward) wind and negative (downwelling) for southerly (northward)

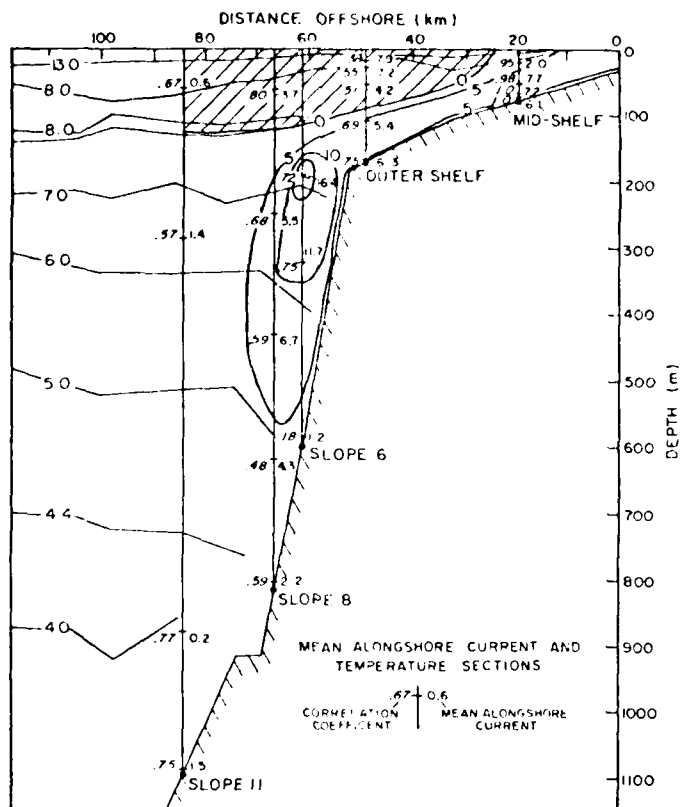


Figure 19. Position of current meter (bar), mean alongshore flow (righthand number) and correlation with the inshore 66 m current record (lefthand number) off southern Washington during the summer of 1972. The data were averaged from 21 July to 28 August. Velocity units are  $\text{cm sec}^{-1}$ . Regions of southward flow are shaded.

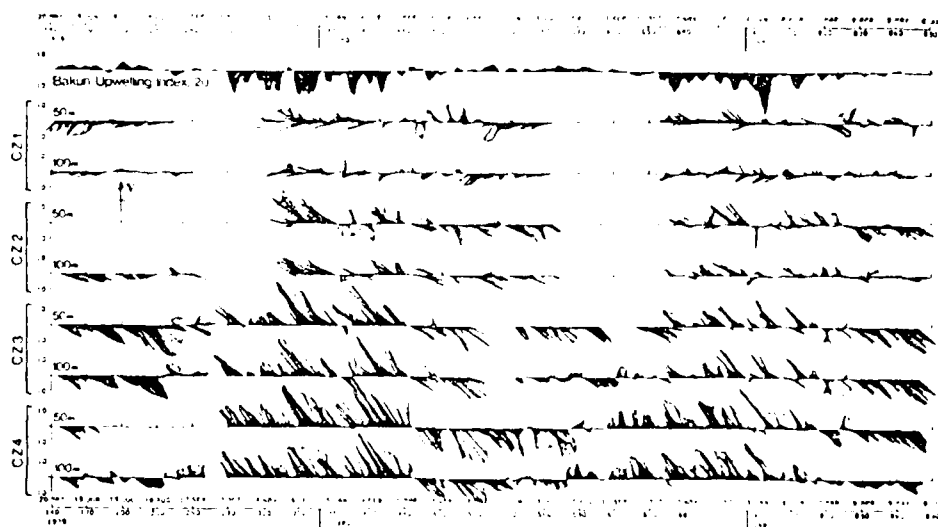


Figure 20. Vector plots of currents at 50 m and 100 m at the four principal mooring sites, and the Bakun Upwelling Index at 48°N 125°W, from 20 May 1979 to 8 June 1981

wind. In this plot only the time series for the currents at 50 and 100 m are shown. Data were also collected from deeper meters at some of the moorings.

The shallow character of these data only reveals the seasonal changes in the near surface current and does not indicate the presence of the CUC. The seasonal shift, in surface current, is very apparent, especially in the two moorings at, or beyond, the shelf break (CZ3, CZ4). As observed by Freeland and Denman (1982) these stronger currents are sharply aligned to the local bathymetry with currents running parallel to the Continental Shelf break. In 1980 the seasonal reversal, from strong northward flow in winter to strong southward flow in spring-summer, took place on March 18, at CZ3, and March 22 at CZ4. The order was not followed in 1981 when both moorings reversed currents at the same time on March 6. In both cases the real shift in the wind field occurs after the change in the currents. Perhaps all that is needed is a decrease in the southerly wind to permit the return of the southward surface current. Freeland and Denman (1982) suggest that the current reversal may signal the arrival of a coastally trapped wave excited by wind shifts farther down the coast. Such shelf waves were also observed by Crawford and Thomson (1982).

The summer presence of the CUC is clearly seen at CZ3 in Figure 21 also taken from Freeland and Denman (1982). Here current records for 50, 100, and 200 m, along with the upwelling index, reveal that in summer and early fall the surface current flows southward, parallel to the coast, while the current at 200 m flows in the opposite direction. It should be noted that velocities, in both directions, are of the same magnitude. The currents at 100 m flow both north and south representing a transition between the top and bottom.

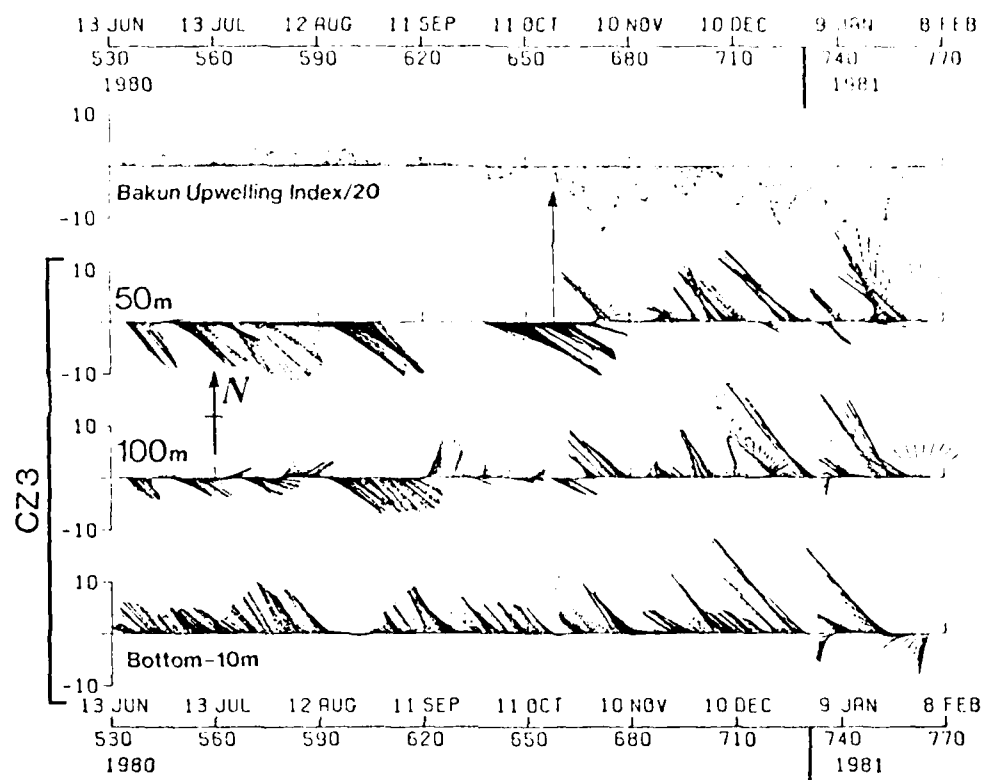


Figure 21. Vector plots of currents at 50 m, 100 m, and 200 m at site CZ3 at the shelf edge to show the presence of a poleward undercurrent during the summer



In mid-October strong downwelling marks the change to southerly wind. A few days later the surface current reverses to flow northward. This northward surface flow continues through the winter while the currents at 100 and 200 m (also northward) intensify. Thus in winter the entire water column flows north as described earlier. The transition to spring conditions was only partially observed, due to equipment problems, but was clearly visible in current meter data collected somewhat farther north off the shelf break.

### Mesoscale Current Variations

(Meanders, eddies, and baroclinic instability)

The various current regimes, off the mouth of Juan de Fuca Strait, give rise to the generation of current meanders due to a mechanism called baroclinic instability. Simply stated this instability mechanism takes energy (both potential and kinetic) out of the mean flow (and the density structure associated with it) and puts it into smaller scale variations with their associated changes in density structure. While this mechanism operates throughout the year, in our region, it is most active in summer-fall when the strong vertical shear feeds the instability. At this time current meanders separate to form separate eddies thus reducing the intensity (and hence instability) of the mean flow.

The surface current meanders manifest themselves in sea surface temperature which can be observed using infrared satellite imagery. Recently Ikeda et al. (1983a) have compared analytical and numerical model results with meander lengths, inferred from infrared satellite imagery, to evaluate the effectiveness of baroclinic instability in generating and maintaining the observed features. They found

that in all three seasons baroclinic instability was operating but particularly unique conditions were seen in summer and fall. During this time of intense vertical shear the satellite observed meanders were either shorter or longer than the wavelength predicted by linear wave theory. Subsequent numerical simulations revealed that the shorter scale meanders were excited by topographic variations in the continental shelf break while nonlinear interactions, between different wavelengths, transferred energy from the shorter scale into one longer than that predicted by the linear results.

The surface temperature patterns associated with these meanders can be clearly seen in the series of infrared satellite images in Figure 22. A reference grid for these and all other images is given in Figure 23. At the start of the series (July 21) the surface temperature off of Vancouver Island is warm everywhere but just off the mouth of Juan de Fuca Strait. As will be discussed more fully later the cold water (lighter shades) at this position indicates the presence of upwelling within a cold cyclonic eddy (Freeland and Denman, 1982) which is driven by the local bottom topography. As shown here this eddy appears to entrain water from Juan de Fuca Strait. It should be noted that this eddy exists in some form in all of the summer-fall imagery.

On July 23 a northerly wind starts to blow resulting in upwelling along the coast and at the Continental Shelf break. This coastal cold water acts as a tracer marking fluctuations in the surface current. Early in the series only three larger scale (~150 km) meanders are observed (Fig. 22b).

Starting on August 22 both longer (~150 km) and shorter (~75 km) scale features are present giving a total of six offshore cold tongues in Figure 22i. As time

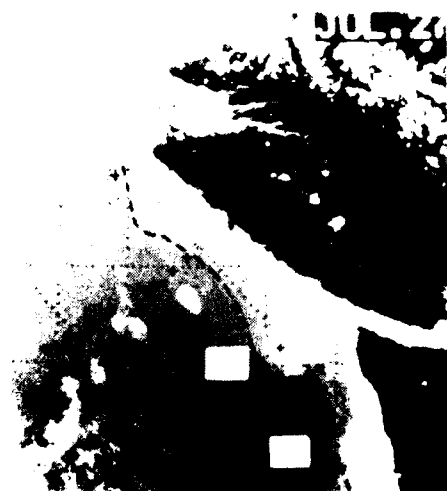
(a)



(b)



(c)



(d)



(e)

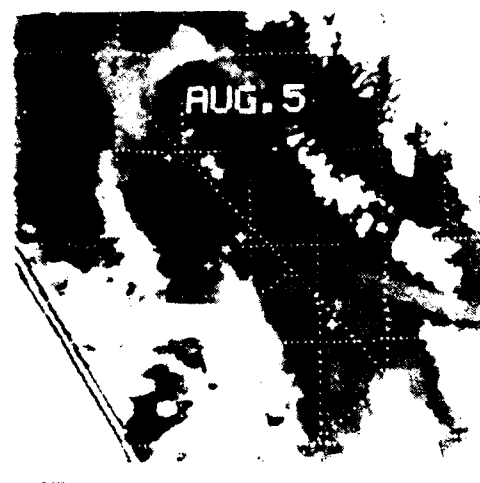
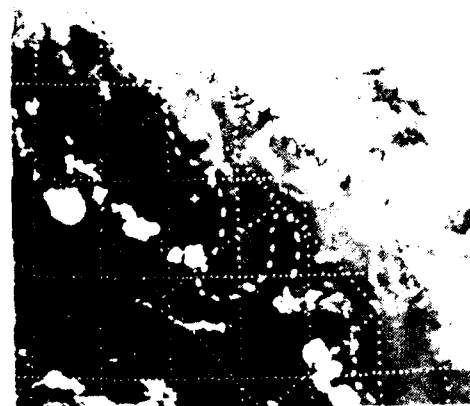


Figure 22. Satellite infrared images taken in the summer and fall of 1961.  
(a) July 21, (b) 27, (c) 28, (d) 30, (e) August 3, (f) 5

(g)



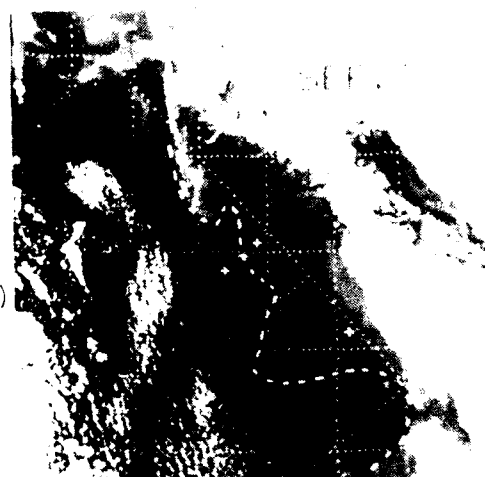
(j)



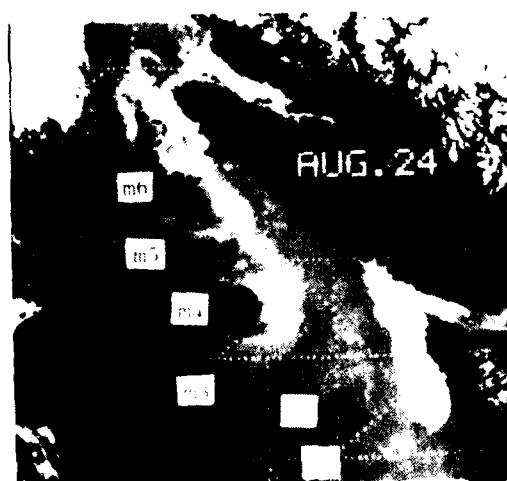
(h)



(k)



(i)



(l)

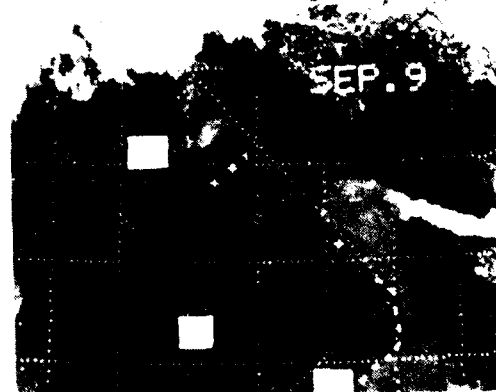
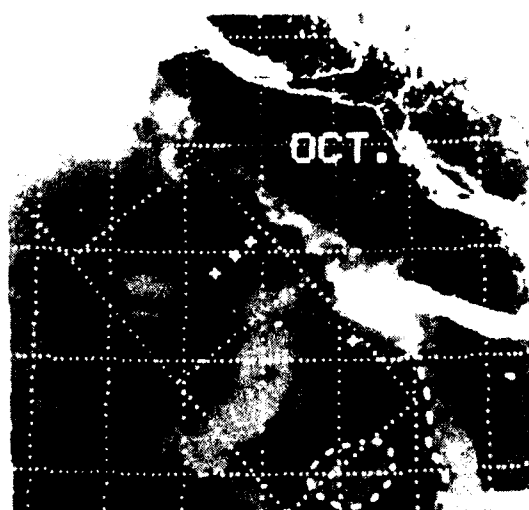


Figure 22. Satellite infrared images taken in the summer and fall of 1980.  
(g) August 11, (h) 22, (i) 24, (j) 28, (k) September 7, (l) 9

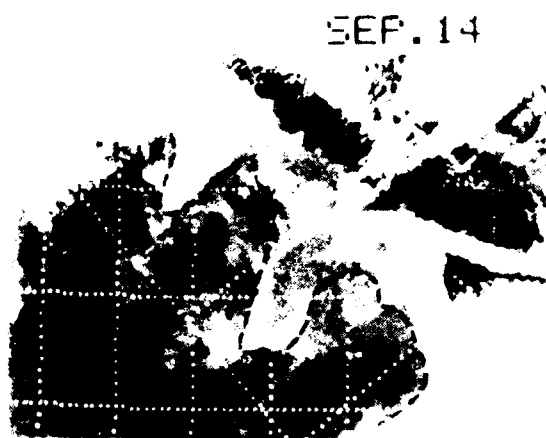
(m)



(o)



(n)



(p)

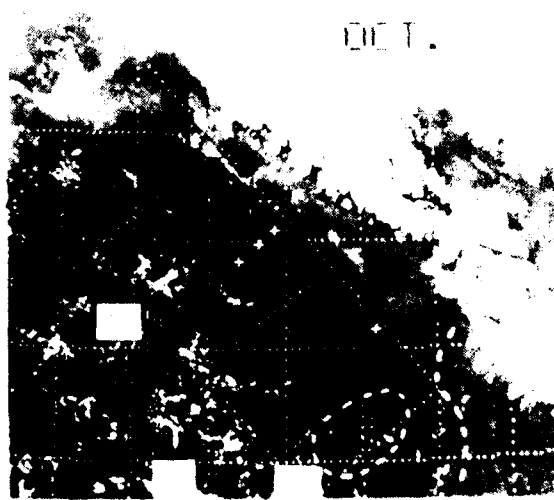


Figure 22. Satellite infrared images taken in the summer and fall of 1980.  
(m) September 12, (n) 14, (o) October 2, (p) 8

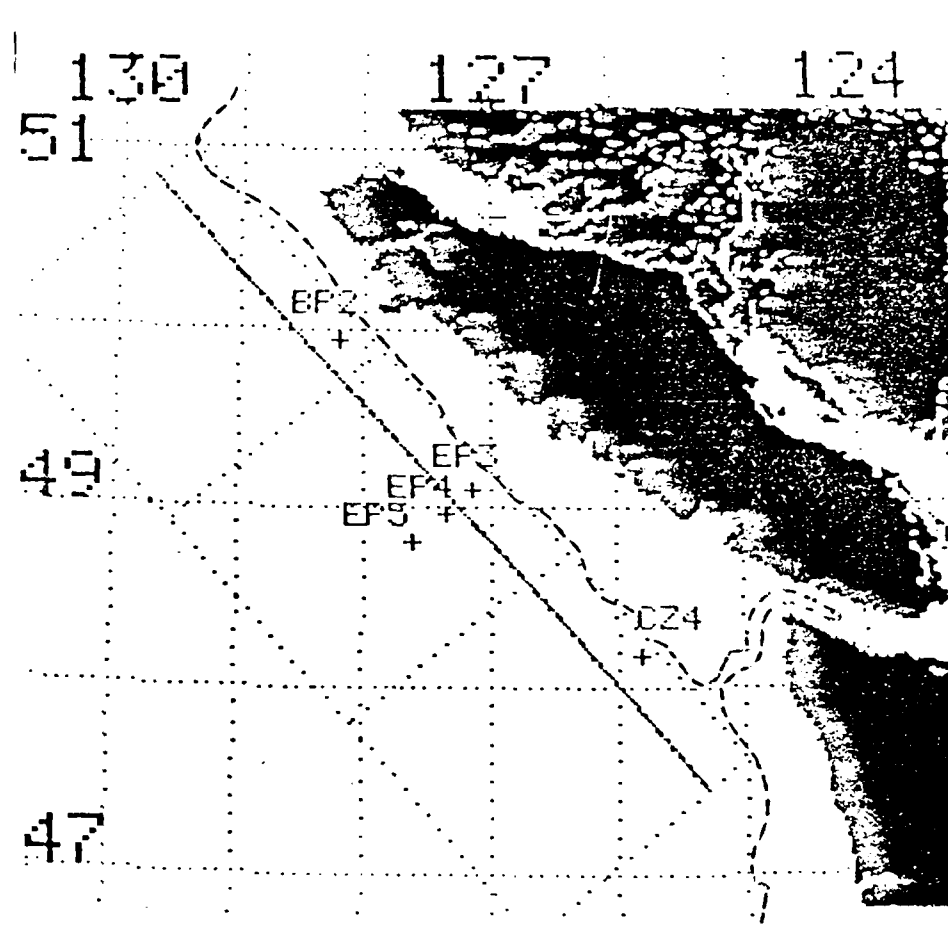


Figure 23. Reference grid for satellite imagery. Solid line indicates the Continental Shelf break. Dashed line is the 183 m contour. Dotted square regions parallel to coastline are numerical model domains. Current meter mooring locations are indicated by plus signs

progresses the smaller scale features weaken while the larger ones grow to eventually, on October 2, separate to form three distinct cold, cyclonic eddies. The larger size of the central eddy is likely related to its position at the terminus of the outflow from Juan de Fuca Strait. That these eddies are not just shortlived transients is evidenced by their continued presence on October 8.

To demonstrate that this series was not just a case of very good luck, another series of infrared satellite images, from the summer-fall of 1982, is shown in Figure 24. Here again a variety of meander scales is apparent on June 24 and August 24. Only a single eddy can be seen in the images from October 12 and 29. Unfortunately poor weather in July and August made it impossible to connect the meander patterns, seen in June, to the eddies observed in October. It is likely that inter-annual (year-to-year) changes in the summer-fall current system could have led to the differences between the 1980 and 1982 satellite image series.

A synopsis of the feature evolution, recorded in the 1980 satellite image series, is given in Figure 25. the transition from the six smaller scale meanders to the three tongues, which then shed eddies, is represented along a time axis. This evolution was modelled using a four-layer numerical model as described in Figure 26. Here the top layer contains the surface current, the second layer the CUC, and the two deeper layers are not in motion but represent stratification differences that provide potential energy to feed into the meanders. The summer vertical shear, as observed in the current meter data, is introduced as the vertical current profiles in Figure 27. The late summer-early fall strengthening of the CUC is well represented. The offshore structures of the idealized surface (SC) and undercurrents (CU) are shown in Figure 28. As has been discussed the CU has been considered symmetrical, while the surface current is shifted towards the shelf-break boundary.

Using this model structure a linear instability analysis was carried out. It suggested that the fastest-growing, maximally unstable wave should have a wavelength near 100 km. This size meander was not observed in any of the satellite imagery. Instead both large (50-km) and short (75-km) scale features were evident in summer infrared sea surface temperature. A nonlinear model, using the same vertical density structure, was initialized with small amplitude meanders of these two scales. The subsequent growth and evolution of these perturbations is shown schematically in Figure 29. Note from initialization to eddy separation took 40 days, about the same period of time as seen in the satellite images from August 22 to October 2. The resultant meander positions and overall size also agree well with the two smaller eddies seen in the satellite imagery. A study of the model energetics revealed how the meanders fed primarily on the potential energy associated with the strong vertical shear.

A subsequent study (Ikeda et al., 1983b) was carried out to determine why 75- and 150-km meanders were observed rather than the ~100-km waves predicted by linear theory. This work revealed that a series of topographic hills and valleys (with about a 75-km spacing) in the continental slope interacted with the undercurrent flow to initiate the shorter scale meanders. Nonlinear interactions then fed energy into the next harmonic scale giving rise to 150-km features. These then grew to dominate the pattern and eventually shed eddies.

Meanders, in infrared sea surface temperature patterns, are still observed in winter (Fig. 30) and spring (Fig. 31) when the entire water column is flowing north or south, respectively. Under these conditions the baroclinic instability mechanism is feeding energy from the mean stratification into the perturbations. It is interesting that the general meander scale, seen in the imagery from both winter and



spring, is about 125 km--the length scale predicted by linear theory for these current structures. Thus only in the presence of the strong vertical shear in summer do nonlinear processes appear to be important in the instability mechanism.

In summary it should be cautioned that in spring and winter 125-km wavelength meanders, of the mean flow, are to be expected in our area of interest. In summer both 75- and 150-km meanders may be encountered in addition to cyclonic eddies separating from the 150-km meanders. Short-lived anti-cyclonic (clockwise) eddies also appear adjacent to the cyclonic cells during the time of formation. Below each of the surface features in summer is a similarly sized feature with the opposite flow direction. Speeds in the meanders and eddies are about the same as those in the mean flow (~20 cm/sec).

### Upwelling

As has been mentioned an important characteristic of the summer flow regime, in this area, is wind-driven upwelling. Many studies, both theoretical and observational, have confirmed and expanded on the idea that an equatorward wind along an eastern boundary will produce offshore transport leading to upwelling along the coast. Depending upon the size and shape of the Continental Shelf this upwelling may take place primarily over the shelf break or strictly off of the land boundary. As brought out earlier, in our region we also have a case of topographically driven upwelling which brings deeper water to the surface even in the absence of the appropriate wind.

Freeland and Denman (1982) identify a cyclonic eddy in the 50/500 m dynamic topography (Fig. 32) as the source of the cold water seen at the same position in

many of the satellite images. They conclude that this eddy is generated by the interaction of the alongshore current with the bottom topography in the form of the Spur Canyon off Juan de Fuca Canyon (Fig. 3). Unlike wind driven upwelling this eddy related cold water is present throughout the summer. Calculations of wind-driven upwelling yield vertical velocities that are smaller than required and a time scale longer than that observed.

This topographically driven eddy can be clearly seen throughout a series of satellite images (Fig. 33) from July-August, 1980 (Ikeda and Emery, 1983). These images document the surface expressions of a wind-driven upwelling event. Initially (July 21) the sea surface off Vancouver Island is warm (dark) except for the cold, cyclonic eddy (just discussed) over the Spur Canyon. Cold water appears to extend west, out of Juan de Fuca Strait, to be entrained in this eddy.

An upwelling-favourable (northwest) wind begins to blow on about July 22. By July 23 a narrow band appears off the coast of Vancouver Island concentrated in the north. On the following day this band has widened and temperatures are lower (brighter). Also on July 24 it is clear that a weaker band of cold water is present just off the Continental Shelf break. Thus it is suggested that upwelling is taking place both at the shelf break and at the coastal boundary. This dual nature is unlike many other upwelling regions which exhibit either shelf break or coastal upwelling but not both. Again the unique character of this region lies in the relatively wide Continental Shelf combined with its open access to upwelling winds.

As the northwest wind strengthens the coastal cold water intensifies and spreads seaward. At the same time the topographic cold eddy appears to increase in

size as wind-driven upwelling is added to it. On July 27 and 28 the cold/warm boundary appears much more meandered than on preceding or succeeding days. By July 30 the coastal cold band has extended beyond the shelf break and now covers the entire Continental Shelf. By August 5 coastal temperatures have started to increase marking the cessation of upwelling. The northwest winds had stopped seven days earlier on July 29 suggesting a spin-down time for an upwelling event.

### Summary

The region of interest (47-49°N, 124-127°W) is influenced both by local and remote forces. External influences are the inflow of fresh water from the Strait of Juan de Fuca, the intrusion of temperature minimum water from the north and west, and the extension of the California Undercurrent into the area, except in spring. Local processes of importance are both wind and topographically produced upwelling and the formation of eddies and meanders through baroclinic instability.

These forces combine to produce the seasonal patterns of mean currents with all southward flow in the spring, southward surface current over a northward undercurrent in summer and fall, and all northward flow in the winter. Meanders, formed by baroclinic instability associated with these current structures, vary from 125-km features in winter and spring to a transition from 75-km to 150-km features in summer. Linear dynamics seem to hold in winter and spring while nonlinear processes are active in summer-fall, when the shorter scale features are stimulated by bottom topography.

In terms of sound velocity the primary concern stems from the intrusions of temperature minima which form shallow surface ducts. Dependent on the vertical



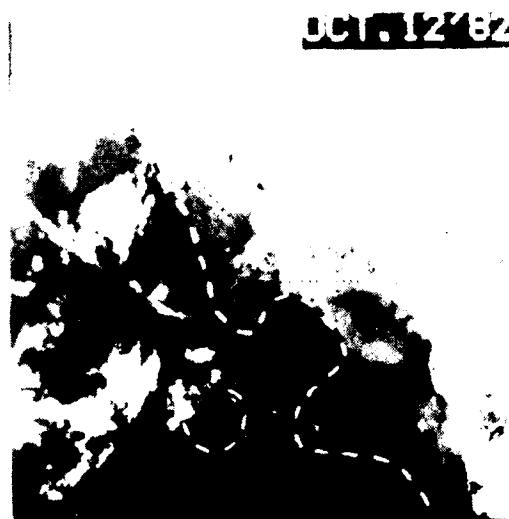
JUN. 18 '82



JUN. 24 '82



OCT. 12 '82



OCT. 29 '82



Figure 24. Series of infrared satellite images from the summer of 1982.  
Dark is warm; light is cold.

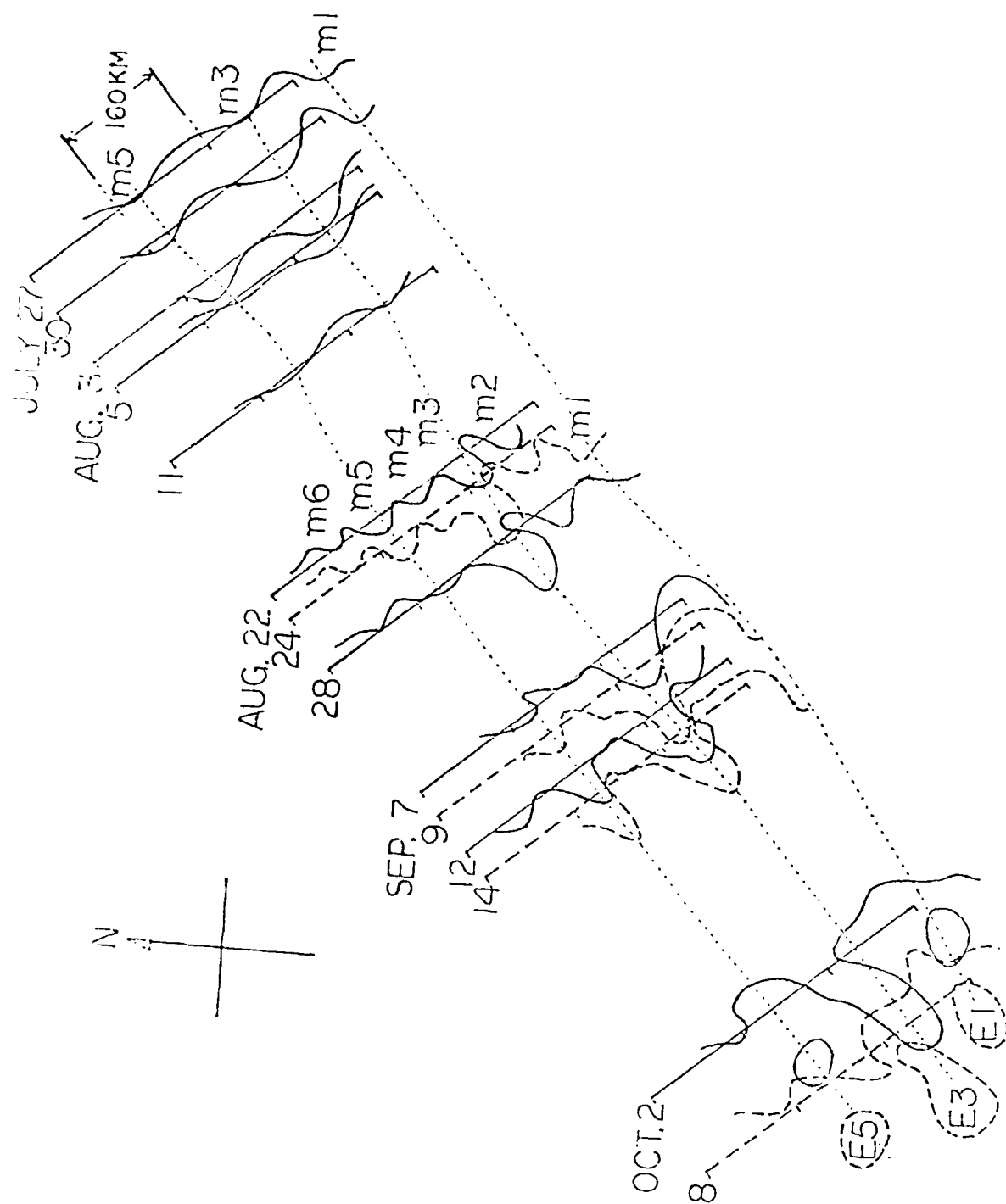


Figure 25. Schematic representation of meander and eddy features observed in satellite images from the summer of 1980

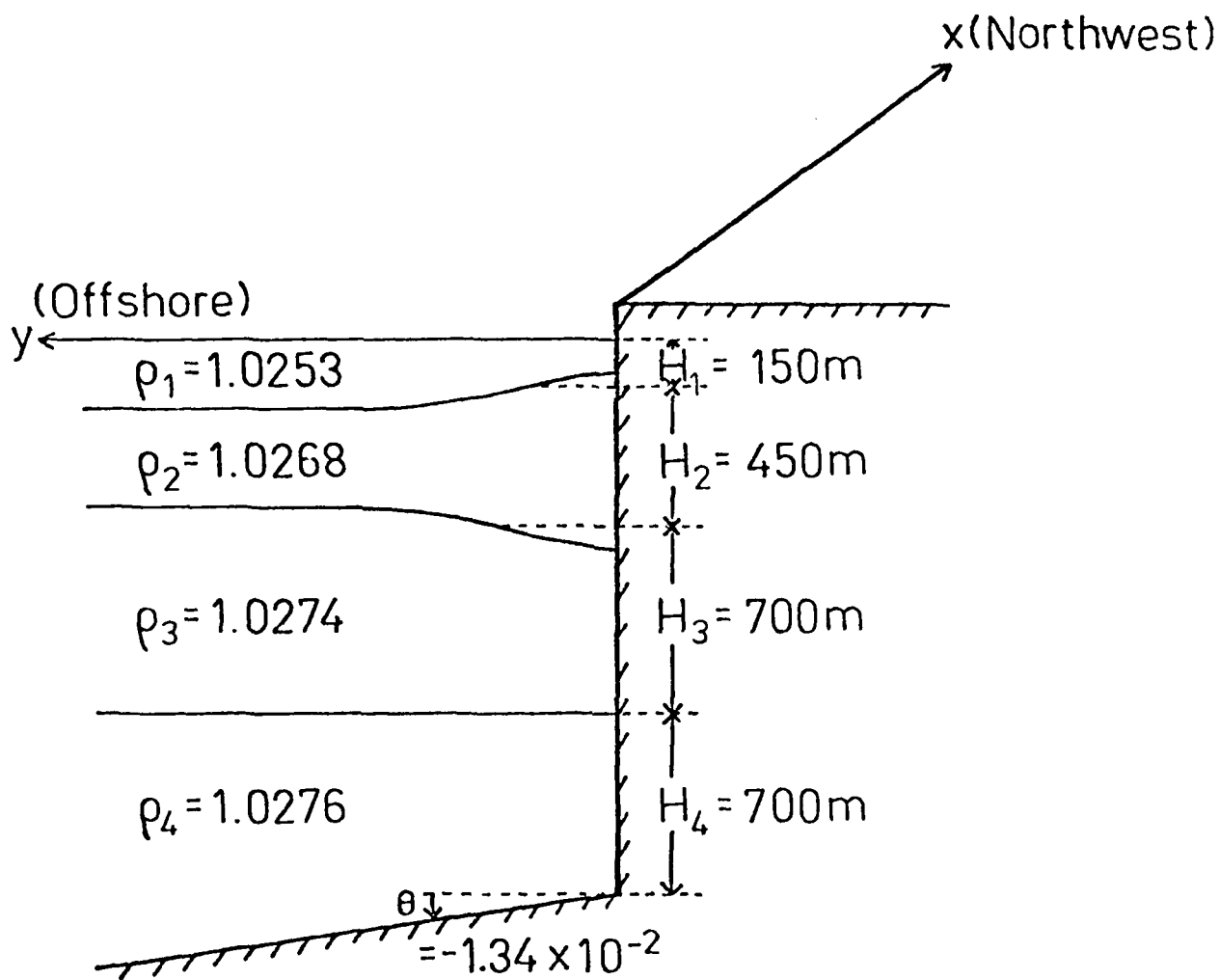


Figure 26. Vertical structure of four-layer model

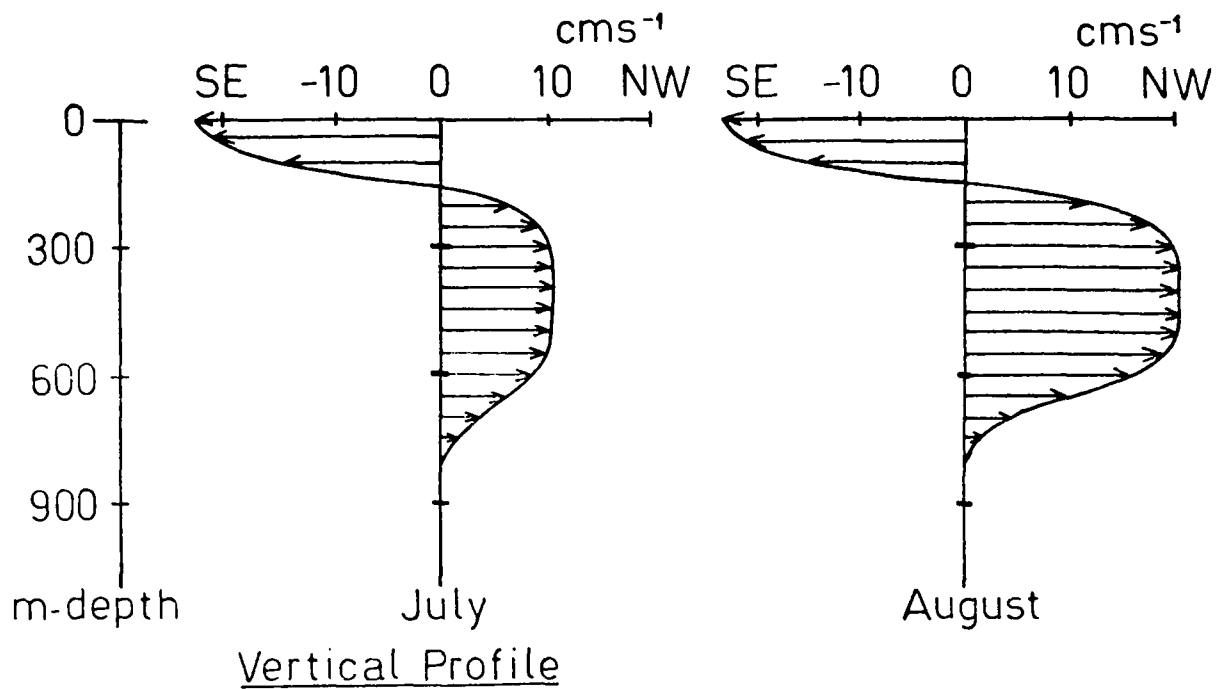


Figure 27. Idealized vertical velocity profiles used in the numerical model

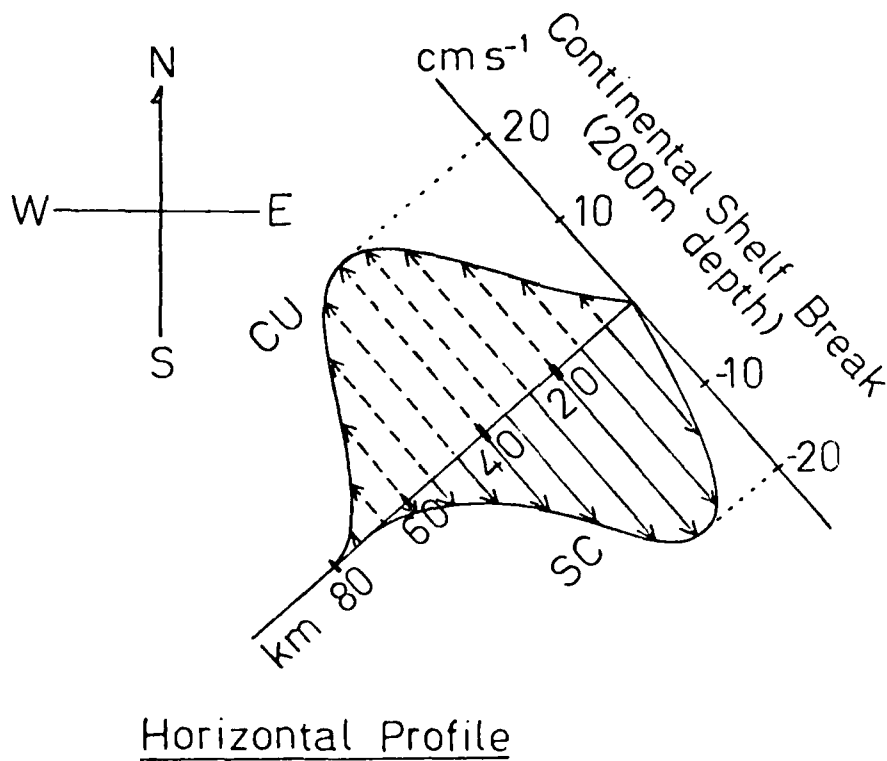


Figure 28. Horizontal structures of currents in the numerical model

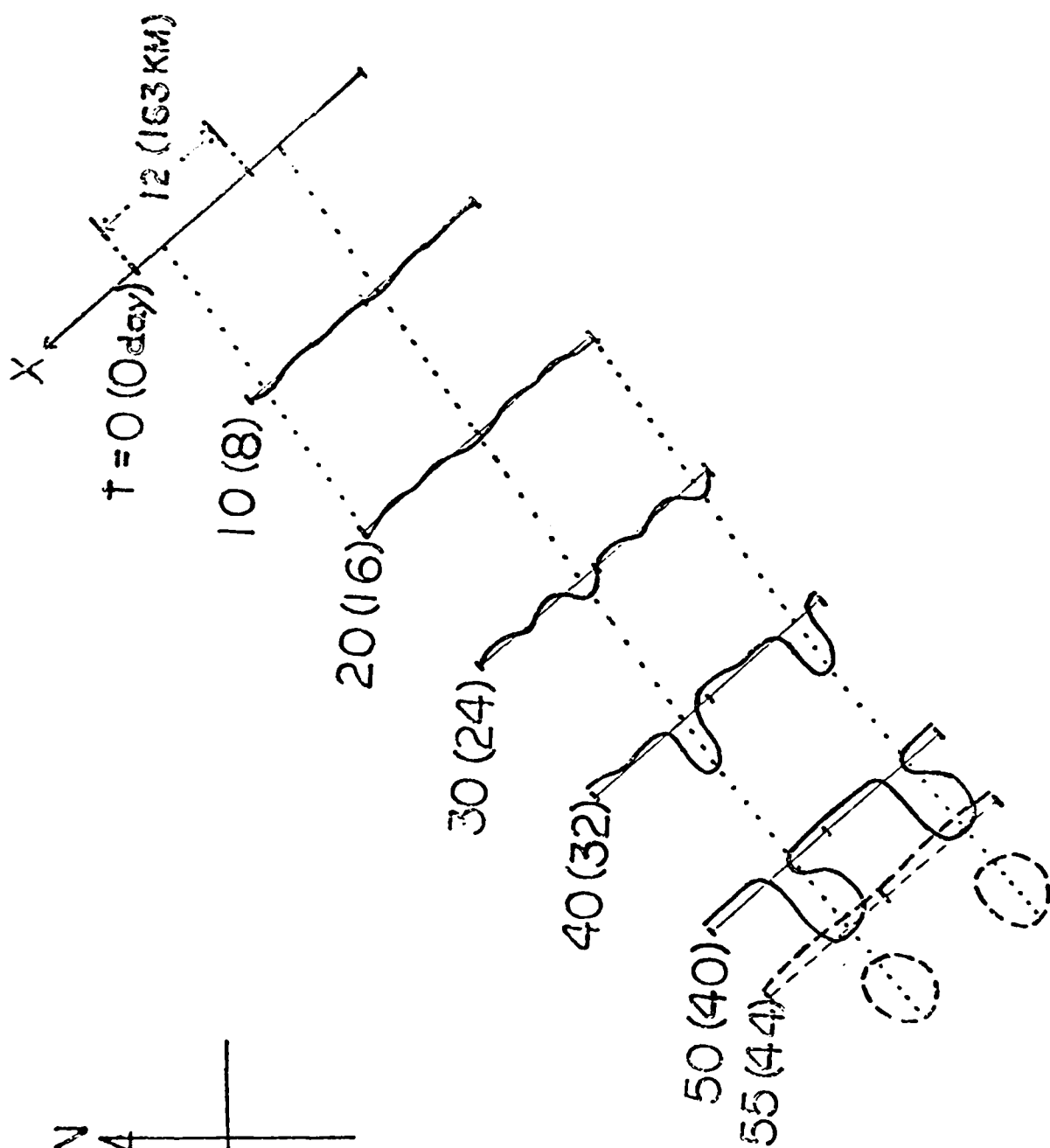
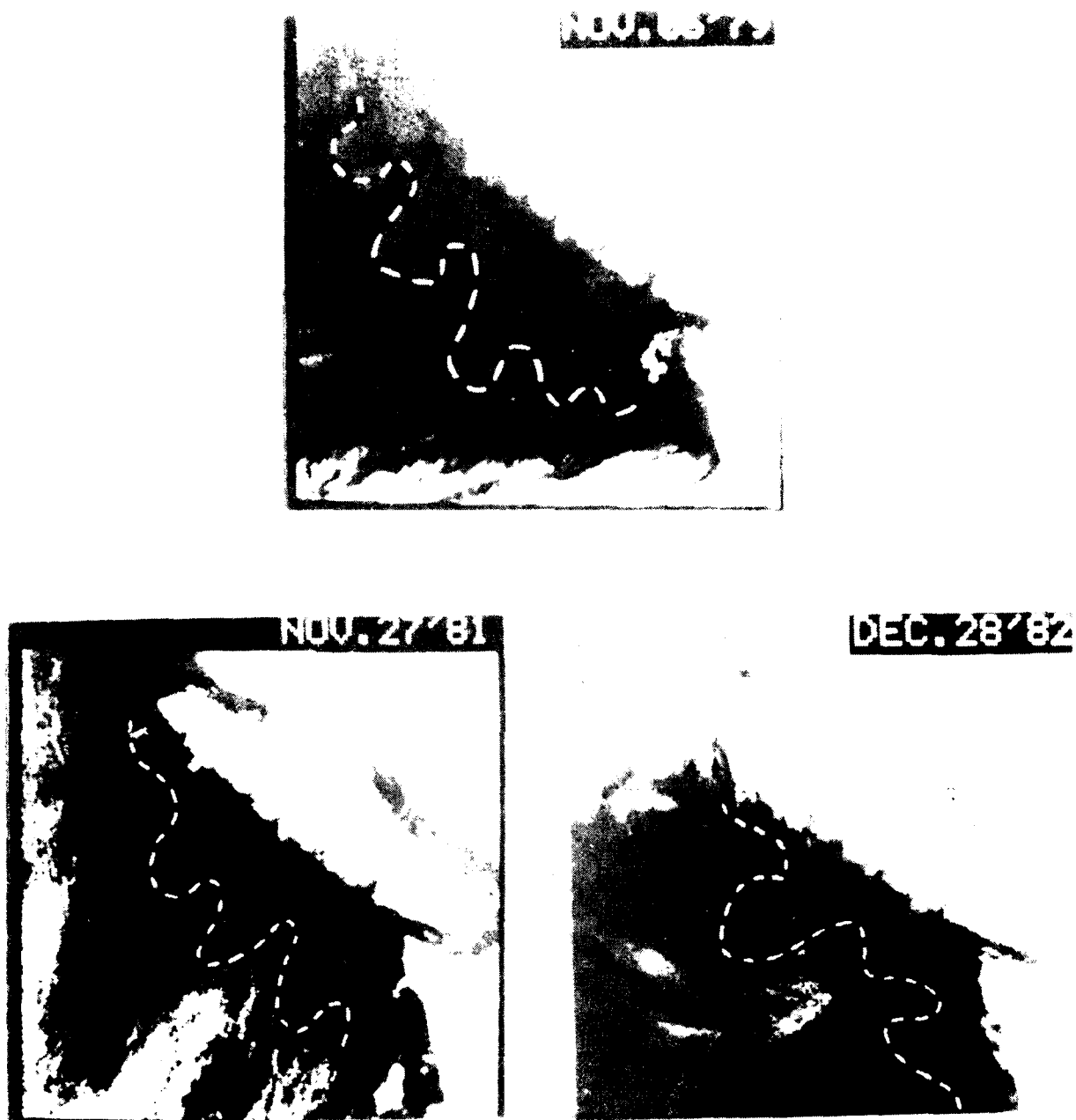
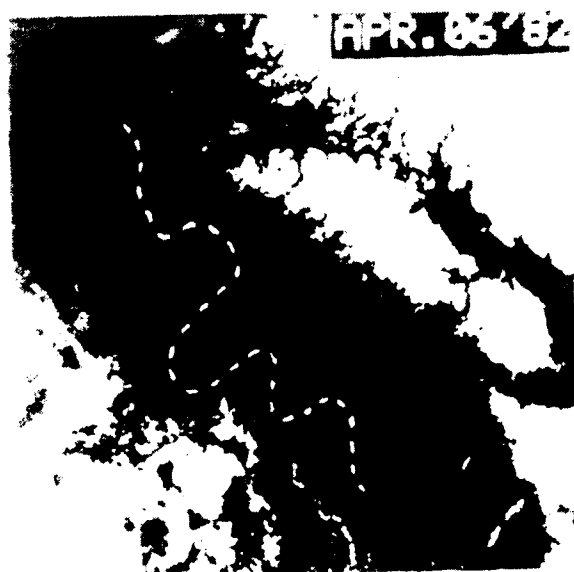
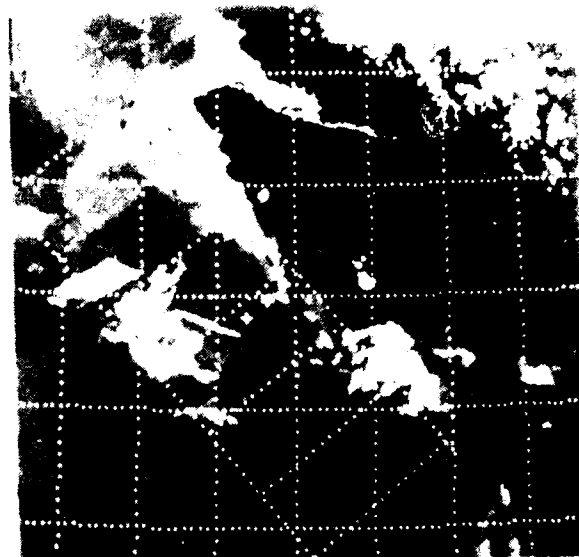


Figure 29. Schematic representation of meander and eddy features simulated by the numerical model





*Figure 30. Winter series of infrared satellite images*



*Figure 31. Spring series of infrared satellite images*

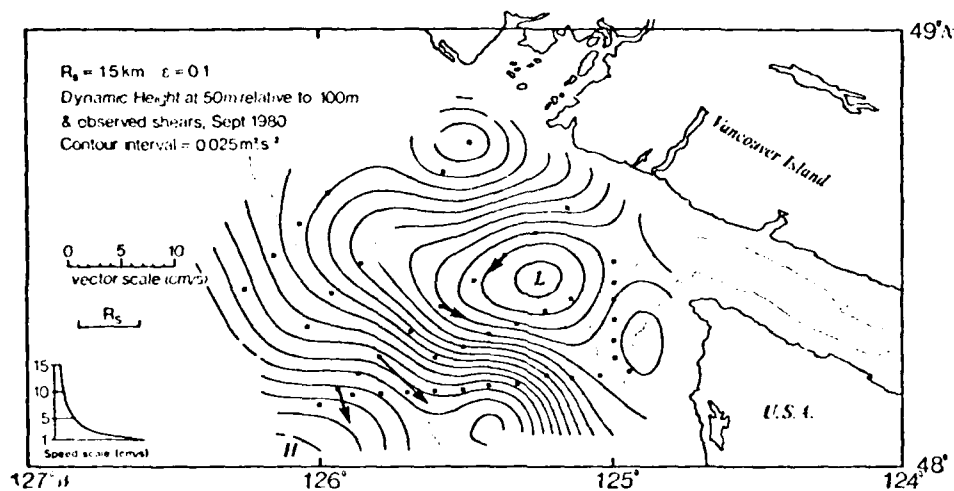
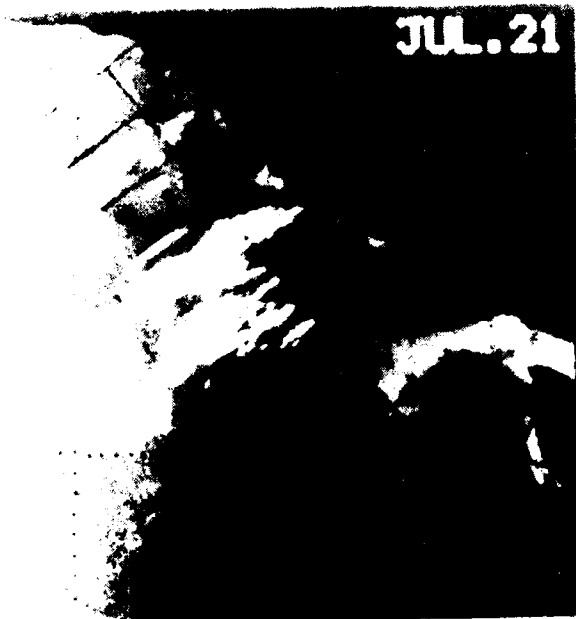


Figure 32. Dynamic height field at 50 m relative to 100 m and the observed shear vectors between 50 and 100 m. Two speed scales are shown, one for the vectors (the linear scale) and one for computing the speeds from contour separations (the nonlinear scale). For further information see caption for Figure 5.



(a)

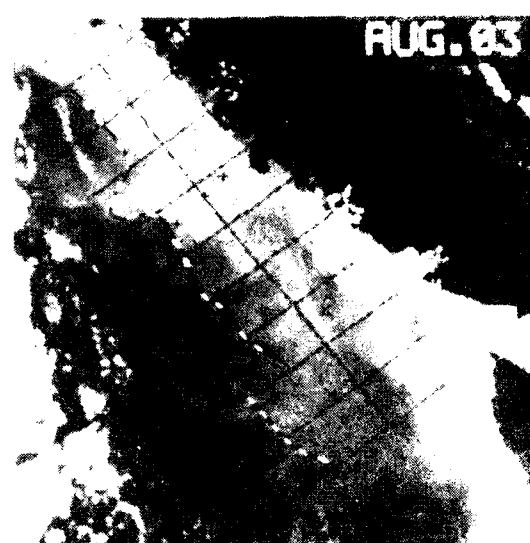
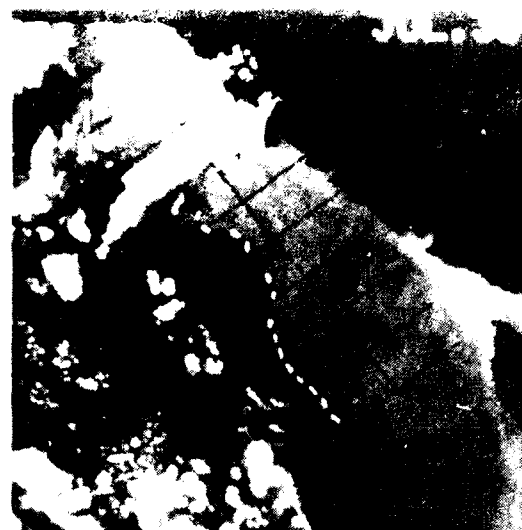


(c)



(b)

Figure 33. Series of infrared satellite images covering an upwelling event in July-August, 1980



salinity structure these minima (and hence sound channels) are usually located between 100 and 200 m coincident with the halocline (maximum salinity gradient). It is unlikely that these features form locally but rather advect into the region from the west and north with the surface current. Thus new temperature minima can only arrive in spring, summer, and early fall when the surface current is southward. In winter flow is everywhere from the south advecting in warm water rather than cold. Temperature maxima, however, are not frequently observed. In winter vertical mixing may also form surface sound velocity ducts.

### References

- Bennett, E. B. (1959). Some Oceanographic Features of the Northeast Pacific Ocean During August 1955. J. Fish. Res. Bd. Canada, v. 16, pp. 565-605.
- Chow, R. K. and D. G. Browning (1983). A Study of Secondary Sound Channels Due to Temperature Inversions in the Northeast Pacific Ocean. Defense Research Establishment Pacific, FMO, Victoria, B.C. (unpublished manuscript).
- Dodimead, A. J., F. Favorite, and T. Hirano (1963). Review of Oceanography of the Subarctic Pacific Region. Bulletin No. 13, Int. North Pac. Fish. Comm., INPFC #546.
- Emery, W. J. and Lt. J. Dewar (1982). Mean Temperature-Salinity, Salinity-Depth, and Temperature-Depth Curves in the North Atlantic and North Pacific. Prog. in Oceanography, n. 3, Pergamon Press, 91 pp.
- Fredland, H. J. and K. L. Denman (1982). A Topographically Controlled Upwelling Center off Southern Vancouver Island. J. Mar. Res., v. 40(4), pp. 1069-1093.

Hickey, B. M. (1979). The California Current System--Hypotheses and Facts. Prog. in Oceanography, n. 4, Pergamon Press, pp. 191-279.

Ikeda, M. and W. J. Emery (1983). An Upwelling Event Observed in Satellite Images Over the Continental Shelf off Vancouver Island (Submitted to J. Mar. Res.).

Ikeda, J., L. A. Mysak, and W. J. Emery (1983a). Observation and Modelling of Satellite-Sensed Meanders and Eddies off Vancouver Island. J. Phys. Oceanogr. (in press).

Ikeda, M., W. J. Emery, and L. A. Mysak (1983b). Seasonal Variability of the Meanders of the California Current System off Vancouver Island (submitted to J. Geophys. Res.).

Lueck, R. G., W. R. Crawford, and T. R. Osborn (1983). Turbulent Dissipation over the Continental Slope off Vancouver Island. (unpublished manuscript)

Roden, G. (1964). Shallow Temperature Inversions in the Pacific Ocean. J. Geophys. Res., v. 69(14), pp. 2899-2913.

Roden, G. (1975). On North Pacific Temperature, Salinity, Sound Velocity and Density Fronts and Their Relation to the Wind and Energy Flux Fields. J. Phys. Oceanogr., v. 5(4), pp. 557-571.

Thomson, R. E. and W. R. Crawford (1982). The Generation of Diurnal Period Shelf Waves by Tidal Currents. J. Phys. Oceanogr., v. 12(7), pp. 635-643.

Tully, J. P., A. M. Dodimead, and S. Tabata (1960). An Anomalous Increase of Temperature in the Ocean off the Pacific Coast of Canada through 1957 and 1958. J. Fish. Res. Bd. Canada, v. 17(1), pp. 61-80.

Wyrтки, K. (1974). The Dynamic Topography of the Pacific Ocean and its Fluctuations. Hawaii Institute of Geophysics, HIG-74-5.



UNCLASSIFIED

SECURITY CLASSIFICATION OF THIS PAGE (When Data Entered)

REPORT DOCUMENTATION PAGE		READ INSTRUCTIONS BEFORE COMPLETING FORM
1. REPORT NUMBER NORDA Technical Note 231	2. GOVT ACCESSION NO.	3. RECIPIENT'S CATALOG NUMBER
4. TITLE (and Subtitle) Physical Oceanography of the Continental Shelf Region off Juan de Fuca Strait		5. TYPE OF REPORT & PERIOD COVERED Final
		6. PERFORMING ORG. REPORT NUMBER
7. AUTHOR(s) William J. Emery		8. CONTRACT OR GRANT NUMBER(s)
9. PERFORMING ORGANIZATION NAME AND ADDRESS Naval Ocean Research & Development Activity Ocean Acoustics and Technology Directorate NSTL, MS 39529		10. PROGRAM ELEMENT, PROJECT, TASK AREA & WORK UNIT NUMBERS
11. CONTROLLING OFFICE NAME AND ADDRESS Naval Ocean Research & Development Activity Ocean Acoustics and Technology Directorate NSTL, MS 39529		12. REPORT DATE May 1984
		13. NUMBER OF PAGES 69
14. MONITORING AGENCY NAME & ADDRESS (if different from Controlling Office)		15. SECURITY CLASS. (of this report) Unclassified
		15a. DECLASSIFICATION DOWNGRADING SCHEDULE
16. DISTRIBUTION STATEMENT (of this Report)  Approved for public release; distribution unlimited		
17. DISTRIBUTION STATEMENT (of the abstract entered in Block 20, if different from Report)		
18. SUPPLEMENTARY NOTES		
19. KEY WORDS (Continue on reverse side if necessary and identify by block number)  topography    halocline    Brunt-Väisälä frequency salinity      thermocline    barocline isothermal    pycnocline		
20. ABSTRACT (Continue on reverse side if necessary and identify by block number) Through interpretation of observations, a review of the water mass structure and circulation of the ocean just west of the Strait of Juan de Fuca was accomplished. The region of interest (47-49°N, 124-127°W) is influenced both by local and remote forces. External influences are the inflow of fresh water from the Strait of Juan de Fuca, the intrusion of temperature minimum water from the north and west, and the extension of the California Undercurrent into the area, except in spring. Local processes of importance are both wind and topographically produced upwelling and the formation of eddies and meanders		

DD FORM 1473  
1 JAN 73

EDITION OF 1 NOV 65 IS OBSOLETE

S N 0102-LF-014-6601

UNCLASSIFIED

SECURITY CLASSIFICATION OF THIS PAGE (When Data Entered)

UNCLASSIFIED

SECURITY CLASSIFICATION OF THIS PAGE (When Data Entered)

through baroclinic instability.

These forces combine to produce the seasonal patterns of mean currents with all southward flow in the spring, southward surface current over a northward undercurrent in summer and fall, and all northward flow in the winter. Meanders, formed by baroclinic instability associated with these current structures vary from 125-km features in winter and spring to a transition from 75-km to 150-km features in summer. Linear dynamics seem to hold in winter and spring while nonlinear processes are active in summer-fall, when the shorter scale features are stimulated by bottom topography.

In terms of sound velocity the primary concern stems from the intrusions of temperature minima which form shallow surface ducts. Dependent on the vertical salinity structure these minima (and hence sound channels) are usually located between 100 and 200 m coincident with the halocline (maximum salinity gradient). It is unlikely that these features form locally but rather advect into the region from the west and north with the surface current. Thus new temperature minima can only arrive in spring, summer, and early fall when the surface current is southward. In winter flow is everywhere from the south advecting in warm water rather than cold. Temperature maxima, however, are not frequently observed. In winter vertical mixing may also form surface sound velocity ducts.

UNCLASSIFIED

SECURITY CLASSIFICATION OF THIS PAGE(When Data Entered)

END

DTIC

9-86